Preprint Cambridge Centre for Computational Chemical Engineering ISSN 1473 – 4273

Kinetic Monte Carlo statistics of curvature integration by HACA growth and bay closure reactions for PAH growth in a counterflow diffusion flame

Gustavo Leon[1,2], Angiras Menon[1], Laura Pascazio[1], Eric J. Bringley[1], Jethro Akroyd[1,2], Markus Kraft[1,2,3]

released: 7 November 2019

[1] Department of Chemical Engineering
and Biotechnology
University of Cambridge
Philippa Fawcett Drive
Cambridge, CB3 0AS
United Kingdom

E-mail: mk306@cam.ac.uk

[2] CARES
Cambridge Centre for Advanced
Research and Education in Singapore
1 Create Way
CREATE Tower, #05-05
Singapore, 138602

[3] School of Chemical
and Biomedical Engineering
Nanyang Technological University
62 Nanyang Drive
Singapore, 637459

Preprint No. 253

Keywords: Kinetic Monte Carlo model, curved PAH, counterflow diffusion flame, seven-member ring formation

Edited by
Computational Modelling Group
Department of Chemical Engineering and Biotechnology
University of Cambridge
Philippa Fawcett Drive
Cambridge CB3 0AS
United Kingdom

E-Mail: c4e@cam.ac.uk
World Wide Web: http://como.ceb.cam.ac.uk/

Abstract

This paper uses a Kinetic Monte Carlo model that includes processes to integrate curvature due to the formation of five- and seven-member rings to simulate polycyclic aromatic hydrocarbons (PAHs) growing in lightly sooting ethylene and acetylene counterflow diffusion flames. The model includes new processes to form seven-member rings via hydrogen-abstraction-acetylene-addition and bay closure reactions on sites containing partially embedded five-member rings. The model additionally includes bay closure and HACA bay capping reactions for the integration of five-member rings. The mass spectra of PAHs predicted by the model are assessed against experimental data, and the distribution of embedded five-member rings and seven-member rings is studied as a function of spatial location, molecule size and frequency of events sampled in the simulation. The simulations show that the formation of seven-member rings and the embedding of five-member rings is a competitive process. Both types of rings are observed more frequently as the simulation proceeds from the fuel outlet towards the stagnation plane. Approximately 15% of the events that integrate curvature resulted in the formation of a seven-member ring coupled to an embedded five-member ring, and the remaining 85% of events embedded five-member rings via the formation of six-member rings. The proportion of PAHs containing embedded five-member rings and/or seven-member rings is observed to be a function of PAH size, passing through a maximum for PAHs containing 15–20 six-member rings. However, the proportion of PAHs containing both types of ring increases with PAH size, where upwards of 10% of PAHs containing at least one five-member ring and 15 or more six-member rings also contain a seven-member ring.

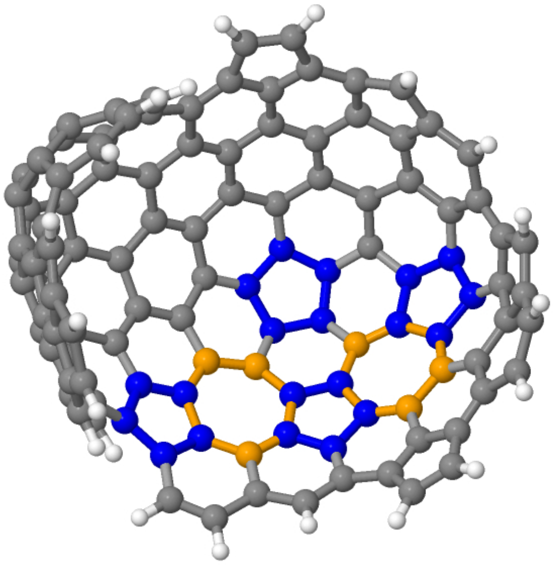

Highlights

- Kinetic Monte Carlo model of PAH growth in counterflow diffusion flames.
- Novel PAH curvature integration jump processes by embedding of five-member rings and by the formation of seven-member rings.
- Spatial distribution and growth statistics of curved molecules are reported.

Contents

1 Introduction

Curvature induced during the growth of polycyclic aromatic hydrocarbons (PAHs) has important consequences for carbon materials. In the case of soot, it has been shown that curved PAHs possess a dipole moment due to the flexoelectric effect [30] that persists at flame temperatures [35]. Such PAHs have been observed in premixed [1, 12] and non-premixed flames [31], and it has been hypothesised that their dipole moments may influence the formation of the first particles [3, 32].

The curvature arises from five- and seven-member rings that are embedded during the growth of a PAH. Five-member rings surrounded by six-member rings results in positive Gauss curvature, corresponding to a bowl-shaped topology. Seven-member rings surrounded by six-member rings results in negative Gauss curvature, corresponding to a saddle-shaped topology.

Five-member rings are found in a variety of carbon materials including nanotubes [29], graphene [46] and fullerenes. Fullerenes have been observed in low pressure benzene flames [10] and have been strongly associated with the presence of curved PAHs [27]. Corannulene (the smallest curved PAH) has been detected in flame-generated soot [27, 58]. High-resolution transmission electron microscopy (HR-TEM) analysis of soot has shown the presence of curved fringes, indicating PAHs containing embedded five-member rings [2, 52]. Partially embedded five-member rings have been directly observed in PAHs using atomic force microscopy, and may be able to lead to fully embedded five-member rings via an acetylene addition step [5].

Seven-member rings have been observed in non-graphitising carbon [16], nanotubes [29] and graphene [41]. The Stone-Wales defect, a double pair of five- and seven-member rings, produces local curvature in graphene [39]. Lines of consecutive five- and seven-member rings have been observed in nanoporous carbons [13], and shown to result in different curvatures in different annealed carbons [33]. In graphene, these lines constitute grain boundaries where the orientation of the carbon atoms change [20]. The partially embedded five-member rings observed by Commodo et al. [5] are contained in bays that provides a site for the formation of a seven-member ring next to the five-member ring.

Kinetic Monte Carlo (KMC) models have been used to simulate PAH growth via the application of a set of transformations and associated rates describing possible growth processes. Frenklach et al. [7] simulated the growth of a graphene edge using the first model that included processes that integrated five-member rings. The model was extended to include five-member ring migration [55], oxygen chemistry that enabled the formation of partially embedded five-member rings [49] and tested under different conditions [56]. Yapp et al. [59] combined a KMC model of the growth of an ensemble of PAHs with a probabilistic model that estimated the Gauss curvature of each PAH as a function of the number of embedded five-member rings.

The above models focused solely on five-member rings as the cause of curvature. The corresponding processes have been studied under a range of conditions. Pope et al. [40] studied the formation of fullerenes via sequential hydrogen-abstraction-acetylene-addition (HACA) and dimerisation reactions. Frenklach and collaborators studied bay capping and competing processes affecting partially embedded five-member rings [8, 60].

Raj [42] investigated the growth of flat and curved PAHs by HACA. However, few studies have considered the formation of seven-member rings. One exception is Kislov et al. [25], who studied a process to create seven-member rings via two HACA additions on a zig-zag site, but found that it was slow relative to other processes.

Recently, Menon et al. [37] calculated rates for the formation of seven-member rings on bay sites containing five-member rings using density functional theory at the M06-2X/cc-PVTZ//B3LYP/6-311+G(d,p) level of theory. The ring formation mechanisms included hydrogen-abstraction-facilitated, hydrogen-addition-facilitated, carbene formation, and direct cyclisation bay closure processes and closure via HACA growth. The calculated rates showed that the formation of seven-member rings by HACA growth and bay closures proceeded at rates similar to the analogous processes for the formation of five and six-member rings.

The purpose of this paper is to study the development of curvature in PAHs due to HACA growth and bay closure reactions in KMC simulations of a counter-flow diffusion flame. The KMC model uses the process rates calculated by Menon et al. [37], for first time enabling simulation of the growth of an ensemble of PAHs that include seven-member rings. The model results are consistent with experimental mass spectra and give insight into the relative abundance and location of PAHs containing embedded five- and seven-member rings.

2 Curvature integration processes

The KMC model used in this work includes two types of process that integrate curvature: The formation of seven-member rings next to existing partially embedded five-member rings and the embedding of five-member rings. These processes are shown in Fig. 1.

Fig. 1(a) and (b) show new processes that form seven-member rings via HACA bay capping. The process in Fig. 1(a) results in a seven-member ring coupled to an embedded five-member ring. The process in Fig. 1(b) results in a seven-member ring coupled to a partially embedded five-member ring. The process rates were taken from Menon et al. [37].

Fig. 1(c) and (d) show new processes for the closure of seven-member bays adjacent to five-member rings. The process rates were taken from Menon et al. [37].

Fig. 1(e) shows a new process that embeds a five-member ring at a six-member bay site that includes a partially embedded five-member ring. There are many possible configurations of such a site. In this work, it was assumed that all configurations proceed at the same rate. The rate is taken by analogy with the most similar process that has been studied in the literature - the closure of a six-member bay site containing only six-member rings. The rate of this process was first calculated by Raj et al. [43]. In this work we repeated the rate calculation at the B3LYP/6-311+G(d,p) level of theory. The process was observed to proceed via hydrogen abstraction (with a barrier in the range 30–35 kcal/mol), or via hydrogen addition, carbene formation or direct cyclisation routes (all with barriers of $\sim$100 kcal/mol). The assumption that this rate can be applied to the process in Fig. 1(e) is made on the grounds that hydrogen abstraction is expected to be the most likely route and is

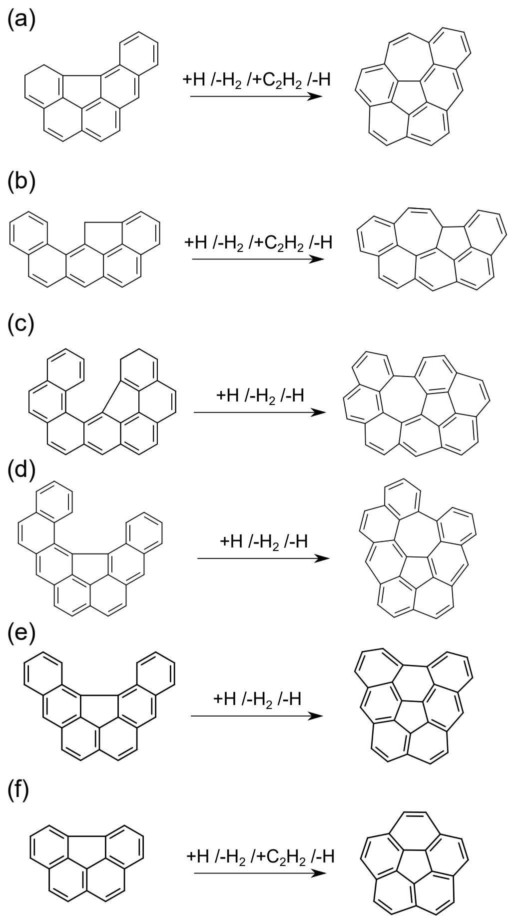

Figure 1: *Curvature integration jump processes.*

expected to have similar rates in both processes, coupled with the observation [37] that the rates of the processes in Fig. 1(a) and (b) are similar and insensitive to the location of the five-member ring, and likewise for the processes in Fig. 1(c) and (d).

Finally, Fig. 1(f) shows a bay capping process that embeds a five-member ring at an armchair site centred on a partially embedded five-member ring. This process is well-known and has been included in previous KMC models. The rate of this process is taken from Raj [42].

Details of the sources for the rates of other processes are provided in the Supplementary Material. Processes that form seven-member rings in the absence of five-member rings are neglected based on the experimental observation that seven-ring member rings are typically found next to five-member rings.

3 Computational method

3.1 Flame model

The ethylene and acetylene counter-flow diffusion flames studied by Skeen et al. [50] were selected as targets for this study. These are lightly sooting flames with faint luminosity on the oxidiser side of the stagnation plane. Similar flames have been used for mass spectrometry studies of radical-radical reactions [23] and the spatial dependence of oxygen substituted compounds [54].

A schematic of the ethylene flame is shown in Fig. 2 (and Fig. S1 for the acetylene flame). The flames were simulated using Cantera [11] with the mechanism of Narayanaswamy et al. [38] to solve the one-dimensional continuity, momentum, species and energy equations.

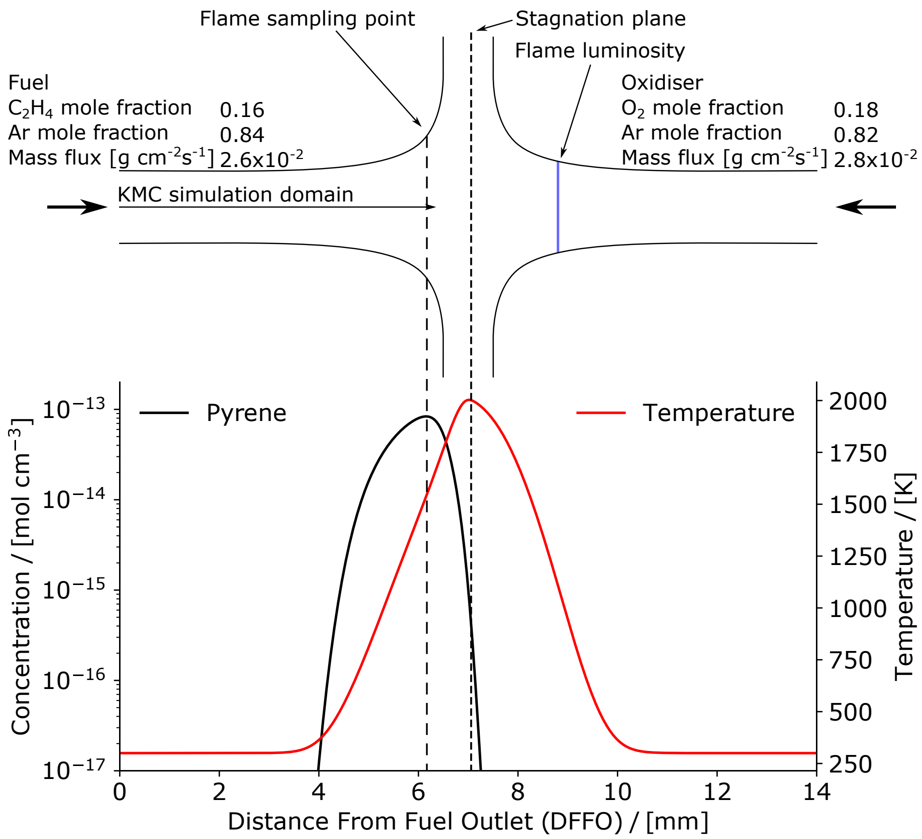

Figure 2: *Schematic of the ethylene flame. The concentration of pyrene and temperature show the flame structure.*

3.2 Kinetic Monte Carlo model

A KMC model was used to simulate the growth of PAHs on the fuel side of the flame. The model tracks the spatial coordinates of the carbon atoms and corresponding reactive sites in each PAH. It uses a combination of the steady-state and partial-equilibrium approximations to estimate the rate of reaction at each site. This treatment of the rates has previously been shown to give good agreement with deterministic simulations of HACA growth [28]. The temperature and species concentrations from the flame simulations (Section 3.1) were provided as boundary conditions to the KMC model, which simulated the growth of PAHs in a Lagrangian control volume travelling from the fuel inlet (DFFO = 0 mm) to just after the sample point (DFFO = 6.17 mm). The PAH growth started from pyrene, the concentration of which was imposed as a boundary condition from the flame simulations. The formation of soot particles was not included in the simulation based on the assumption that the PAH growth is dominated by gas-phase reactions, consistent with the selection of lightly sooting flames with faint luminosity.

4 Results

4.1 Mass spectra

Fig. 3 shows simulated mass spectra for the acetylene and ethylene flames versus corresponding experimental data. The peaks heights are scaled to match at m/z=202, corresponding to imposing the pyrene concentration as a boundary condition. The maximum number of PAHs in the simulations was 14,060 and 81,500 respectively.

The simulations reproduce the relative abundance of the major peaks reasonably well for the acetylene flame. The level of agreement is less certain for the ethylene flame, where the experimental data are only available up to $m/z = 310$. In both cases, and in particular the ethylene flame, the simulations underpredict the peaks for small PAHs, for example at $m/z = 226$. This highlights a potential gap in the current modelling approach, where the growth of multiple small PAHs is simulated in the gas-phase chemical mechanism, and then re-simulated rather than imposed in the KMC simulation.

A number of peaks are missing from the simulated spectra. There are several reasons for this. Firstly, some experimentally observed phenomena including methyl-addition [14], oxygenated species [21, 54], and isotopes [47] are neglected in the current model. Secondly, the model simulates the growth of PAHs from a single species - pyrene. Given that all the remaining growth processes add two carbons, the simulated spectra currently only include even-carbon-numbered species.

4.2 Integration of five- and seven-member rings

Fig. 4 shows the spatial distribution of PAHs containing five- and seven-member rings in the ethylene flame. The temperature and residence time both contribute to observed distribution and it is not possible to separate each contribution within the current study.

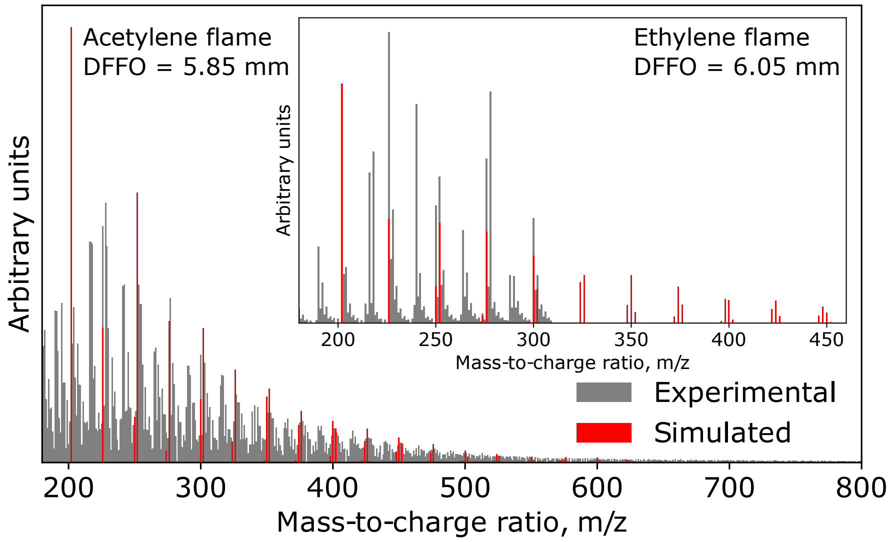

Figure 3: *Simulated and experimental [50] mass spectra for the acetylene (main) and ethylene (inset) flames.*

The first PAHs with one embedded five-member ring are observed at DFFO $\approx$ 5.7 mm. The concentration of these PAHs increases throughout the remainder of the simulation domain. The subsequent addition of five- and seven-member rings occurs via competitive processes that embed a five-member ring either by adding a six- or seven-member ring. Strong correlation is observed between the concentrations of PAHs with two-embedded five member rings and one seven-member ring. Likewise the concentrations of PAHs with four embedded five-member rings and PAHs with two seven-member rings. By the end of the simulation domain, a few PAHs containing up to six embedded five-member rings or four seven-member rings can be observed.

Fig. 5 presents a flux diagram showing the relative sampling frequency of the processes that integrate curvature in the ethylene flame. The most frequent processes are HACA (1(f), 47.4%) and bay closure (1(e), 37.3%) processes that embed five-member rings by adding six-member rings. These occur with similar frequencies. The rate of the bay closure processes is surprisingly high, but can be explained by the nature of the partially embedded five-member ring. Unlike partially embedded five-member rings in armchair sites, which may migrate and desorb [55], bay sites containing partially embedded five-member rings do not allow such migration. Once a bay site containing partially embedded five-member ring appears, it is likely to close and embed the five-member ring.

Both bay closure (1(c) and 1(d), 8.4%) and HACA (1(a), 1.0%) processes simultaneously embed five-member rings by adding seven-member rings. In this case, the rate of the bay closure is considerably higher than the HACA processes. This is attributed to the inability of a partially embedded five-member ring to migrate from a bay, as above. The remainder of the seven-member ring additions occur via HACA (1(b), 3.6%), two thirds of the time followed by the embedding of a five-member ring (1(f), 2.3%).

4.3 Assessing PAH curvature

The probabilistic model by Yapp et al. [59] estimated the Gauss curvature as a function of the number of embedded five-member rings and six-member rings in a PAH. However, the presence of coupled five- and seven-member rings that share a common bond result in a molecule that is nearly flat [39], violating the assumptions made in the probabilistic model. The introduction of processes that integrate coupled five- and seven-member rings in this work allows us to assess the proportion of PAHs for which this occurs.

To assess this, Fig. 6 shows the distributions of the number of PAHs containing different numbers rings at the end of the simulation domain in the ethylene flame. Most of the small PAHs are completely flat. This is expected because a minimum number of five six-member rings needed to embed a five-member ring. The maximum proportion of PAHs with one embedded five-member ring occurs in PAHs with around 15 six-member rings. This maximum is accompanied by a significant growth in the proportion of PAHs with a second embedded five-member ring. This delayed increase in the number of PAHs that contain a second embedded five-member ring is due to the isolated pentagon rule [26]: adjacent five-member rings are not allowed. This reduces the degrees of freedom when trying to embed a second five-member ring. The maximum proportion of PAHs with seven-member rings occurs in PAHs with ~20 six-member rings. The reduction in the proportion of PAHs containing ether five- or seven-member rings in large PAHs follows the overall trend in the total number of PAHs.

Overlaid on Fig. 6(a) is a scatter plot of the proportion of PAHs with at least one embedded five-member ring that also contain a seven-member ring, $\phi_{7|5}$. These PAHs violate the assumptions in the probabilistic model by Yapp et al. [59]. The data become noisy as the number of five-member rings in large species (containing more than 35 six-member rings)

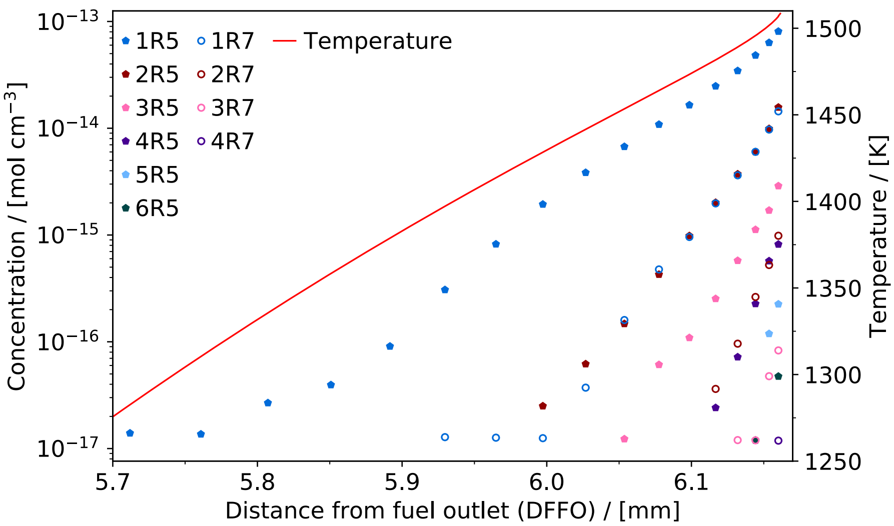

Figure 4: *Spatial distribution of temperature and of PAHs containing five- and seven-member rings in the ethylene flame. nR5 denotes PAHs containing exactly n embedded five-member rings; nR7 denotes exactly n seven-member rings (embedded or otherwise).*

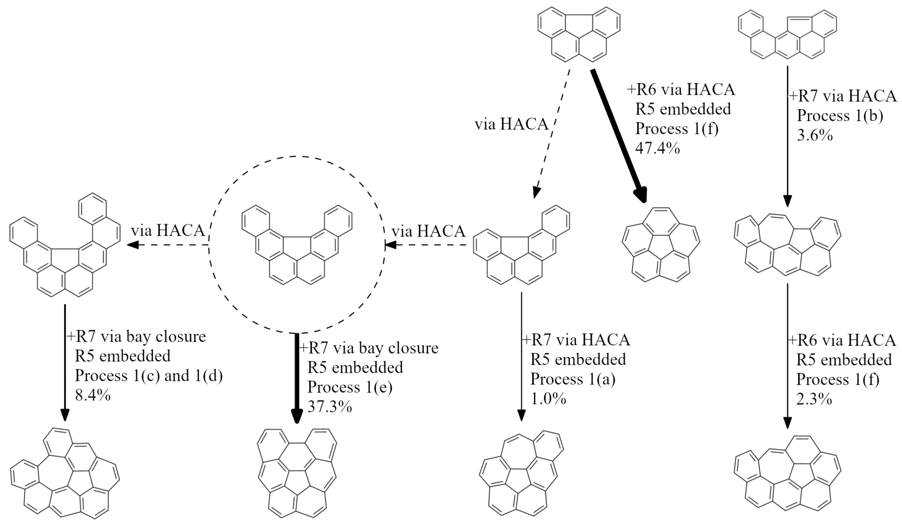

Figure 5: *Flux diagram showing the sampling frequency of processes that integrate curvature in the ethylene flame. The solid arrows show processes that integrate curvature. The percentages show the relative sampling frequency of each process. The dashed arrows show processes that add carbon.*

decreases. It is observed that the larger a PAH containing an embedded five-member ring, the more likely it is to include a seven-member ring.

The same trend is observed in the proportion of PAHs with at least one seven-member ring that also contain at least one embedded five-member ring, $\phi_{5|7}$ shown in Fig. 6(b). The larger a PAH containing a seven-member ring, the more likely it is to include a embedded five-member ring. It is also observed that a proportion of PAHs that contain seven-member rings contain no embedded five-member rings. These result from the HACA growth of seven-member rings on partially embedded five-member rings (Fig. 5, Process 1(b), 3.6%). These five-member rings are eventually embedded as PAHs grows, until all PAHs that contain seven-member rings also contain embedded five-member rings in PAHs with more than 30 six-member rings.

5 Conclusions

A KMC model that, for the first time, includes processes to integrate curvature due to the formation of coupled five- and seven-member rings has been used to simulate PAHs growing in ethylene and acetylene counterflow diffusion flames. The simulation results reproduce the major peaks and relative abundances of experimental mass spectra. Including more processes and an more intimate coupling with the gas-phase would allow the simulation of peaks that are currently missing from the simulated spectra.

The addition of five- and seven-member rings occurs via competitive processes HACA and bay closure processes. It was observed that approximately 85% of the events that integrate curvature correspond to the embedding of five-member rings via the formation of

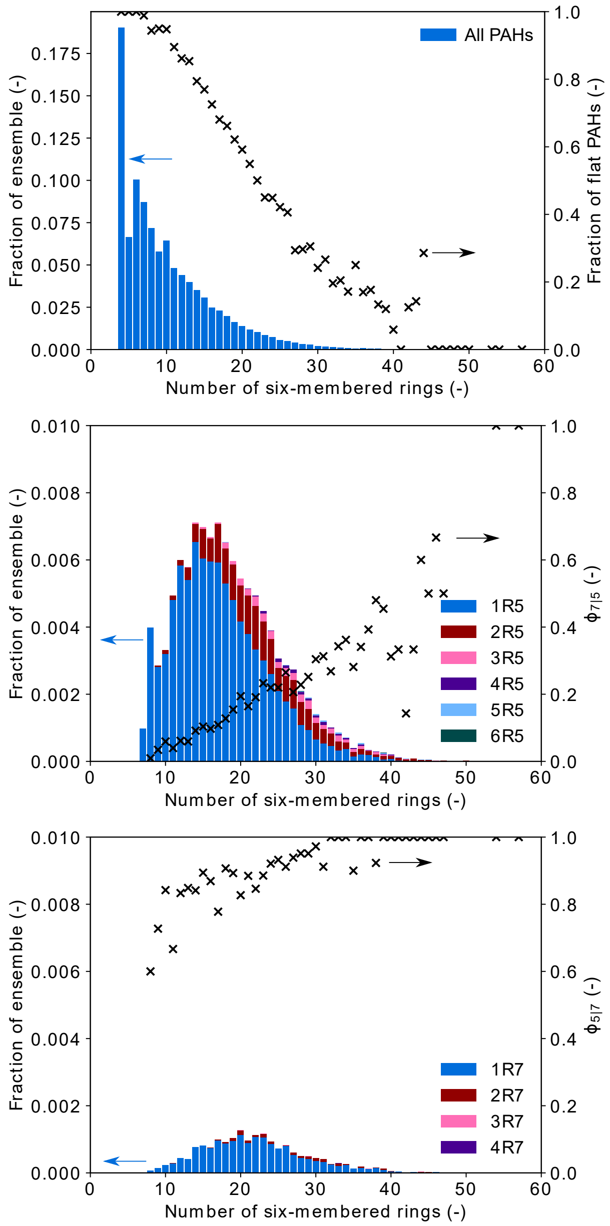

Figure 6: *Histograms showing the distributions of the number of five- and seven-member rings as a function of the number of six-member rings in PAHs in the ethylene flame. The proportion of PAHs with a j-member ring that also contain an i-member ring is denoted $\phi_{i|j}$. nR5 denotes PAHs containing exactly n embedded five-member rings; nR7 denotes exactly n seven-member rings (embedded or otherwise). DFFO = 6.17 mm.*

six-member rings, with HACA and bay closures occurring in similar proportions. The remaining 15% correspond to the formation of seven-member rings coupled to five-member rings, with bay closures occurring approximately twice as often as HACA.

The proportion of PAHs at the end of the simulation domain containing embedded five-member rings and/or seven-member rings is observed to pass through a maximum for PAHs containing ∼20 six-member rings. The proportion that contains both five- and seven-member rings increases with PAH size. The assumption that the PAHs contain only five and six-member rings made in the probabilistic model introduced by Yapp et al. [59] is increasingly violated as the PAHs increase in size.

The development of a KMC model that includes processes to describe the formation of five- and seven-member rings by HACA and bay closure processes provides a starting point for future work to model the cross-linking of PAHs. Cross-linking has been suggested to be important for soot formation [17], including specific suggestions about the role of aryl-crosslinks [19], rim-based five-member rings [6], resonantly stabilised radicals [22] and localised π-radicals [34]. Such cross-linking is expected to create bay sites that require the growth processes implemented in this work.

6 Acknowledgements

This work was partly funded by the National Research Foundation (NRF), Prime Minister's Office, Singapore under its CREATE programme. GL is funded by a CONACYT Cambridge Scholarship and wishes to acknowledge the National Council of Science and Technology and the Cambridge Commonwealth Trust. AM gratefully acknowledges Johnson Matthey for financial support. EB was funded by a Gates Cambridge Scholarship (OPP1144). MK gratefully acknowledges the support of the Alexander von Humboldt foundation.

Supplemental Material

S1 Schematic of the acetylene flame

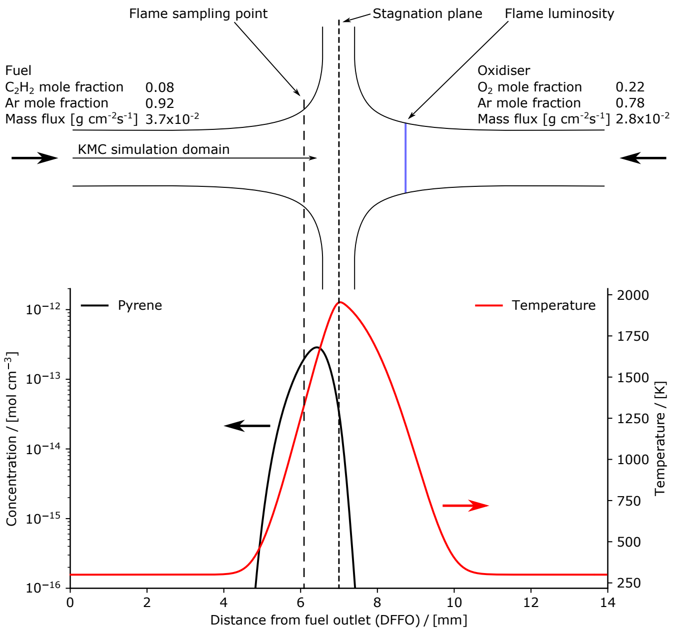

Figure S1: *Schematic of the acetylene flame. The concentration of pyrene and temperature show the flame structure.*

S2 KMC processes rates

Sections S2.1 and S2.2 provide the elementary reaction rate coefficients and the list of jump processes used in the model and their assumptions.

S2.1 List of Kinetic Monte Carlo jump processes

Table S1: *Elementary reaction rate coefficients*

No.	Reactions	$k = AT^n \exp(-E/RT)^a$ A	n	E	References
	Hydrogen abstraction from six-member rings				
1	$C_sR_6{-}H + H \rightarrow C_sR_6^\bullet + H_2$	4.570×10^{08}	1.880	14.839	[48]
-1	$C_sR_6^\bullet + H_2 \rightarrow C_sR_6 + H$	1.690×10^{04}	2.620	4.559	[48]
2	$C_sR_6{-}H + OH \rightarrow C_sR_6^\bullet + H_2O$	5.190×10^{03}	3.040	3.675	[24]
-2	$C_sR_6^\bullet + H_2O \rightarrow C_sR_6 + OH$	5.590×10^{00}	3.573	8.659	[24]
3	$C_sR_6^\bullet + H \rightarrow C_sR_6{-}H$	4.170×10^{13}	0.150		[15]
	Hydrogen abstraction from five-member rings				
4	$C_sR_5{-}H + H \rightarrow C_sR_5^\bullet + H_2$	4.890×10^{09}	1.508	19.862	[18]
-4	$C_sR_5^\bullet + H_2 \rightarrow C_sR_5 + H$	5.068×10^{04}	2.445	4.520	[18]
5	$C_sR_5{-}H + OH \rightarrow C_sR_5^\bullet + H_2O$	5.190×10^{03}	3.040	3.675	[24]
-5	$C_s^\bullet + H_2O \rightarrow C_s + OH$	5.590×10^{00}	3.573	8.659	[24]
6	$C_sR_5^\bullet + H \rightarrow C_sR_5{-}H$	6.080×10^{12}	0.270		[55]
	Hydrogen addition to five-member rings				
7	$C_sR_5H{-}C_sR_5H + H \rightarrow C_sR_5H_2{-}C_sR_5H^\bullet$	5.400×10^{11}	0.450	1.820	[55]
-7	$C_sR_5H_2{-}C_sR_5H^\bullet \rightarrow C_sR_5H{-}C_sR_5H + H$	3.015×10^{11}	0.450	-33.367	[55]
8	$C_sR_5H_2{-}C_sR_5H^\bullet + H \rightarrow C_sR_5H{-}C_sR_5H + H_2$	2.000×10^{12}			[55]
	Armchair growth				
9	$C_sR_6^\bullet + C_2H_2 \rightarrow C_sR_6{-}R_6 + H$	1.190×10^{22}	-2.450	18.890	[9]
10	$C_sR_6^\bullet + C_2H_2 \rightarrow C_sR_6{-}R_6 + H$	1.060×10^{14}	-0.490	8.204	[9]
11	$C_sR_6^\bullet + C_2H_2 \rightarrow C_sR_6{-}C_2H + H$	4.240×10^{14}	0.025	33.080	[9]
12	$C_sR_6^\bullet + C_2H_2 \rightarrow C_sR_6{-}C_2H + H$	7.640×10^{-2}	3.950	16.495	[9]
	Free-edge desorption to produce an armchair				
-9	$C_sR_6{-}R_6 + H \rightarrow C_sR_6^\bullet + C_2H_2$	5.465×10^{30}	-3.657	86.240	[9, 38]
-10	$C_sR_6{-}R_6 + H \rightarrow C_sR_6^\bullet + C_2H_2$	4.868×10^{22}	-1.697	75.550	[9, 38]
	Free-edge ring growth and desorption				
13	$C_sR_6^\bullet + C_2H_2 \rightarrow C_sR_6{-}C_2H_2$	1.910×10^{61}	-14.600	28.610	[36]
-13	$C_sR_6{-}C_2H_2 \rightarrow C_sR_6^\bullet + C_2H_2$	2.499×10^{69}	-16.430	71.290	[36]
14	$C_sR_6^\bullet + C_2H_2 \rightarrow C_sR_6{-}C_2H + H$	1.100×10^{31}	-4.830	26.620	[36]
-14	$C_sR_6{-}C_2H + H \rightarrow C_sR_6^\bullet + C_2H_2$	2.542×10^{37}	-6.213	37.610	[36]
15	$C_sR_6^\bullet + C_2H_2 \rightarrow C_sR_6{-}C_2H_3^\bullet$	1.360×10^{75}	-18.400	40.880	[36]
-15	$C_sR_6{-}C_2H_3^\bullet \rightarrow C_sR_6^\bullet + C_2H_2$	4.055×10^{82}	-20.120	79.400	[36]
16	$C_sR_6^\bullet + C_2H_3 \rightarrow C_sR_6{-}C_2H_3$	6.000×10^{12}			[38]
-16	$C_sR_6{-}C_2H_3 \rightarrow C_sR_6^\bullet + C_2H_2$	8.216×10^{23}	-2.162	119.100	[38]
17	$C_sR_6^\bullet + C_2H_4 \rightarrow C_sR_6 + C_2H_3$	9.450×10^{-3}	4.470	4.472	[38]
-17	$C_sR_6 + C_2H_3 \rightarrow C_sR_6^\bullet + C_2H_4$	2.316×10^{-2}	4.416	6.709	[38]
18	$C_sR_6^\bullet + C_4H_4 \rightarrow C_sR_6{-}R_6 + H$	1.260×10^{04}	2.610	1.434	[38]
-18	$C_sR_6{-}R_6 + H \rightarrow C_sR_6^\bullet + C_4H_4$	1.130×10^{16}	0.754	66.940	[38]
19	$C_sR_6 + C_2H_3 \rightarrow C_sR_6{-}C_2H_3 + H$	1.870×10^{07}	1.470	5.533	[38]
-19	$C_sR_6{-}C_2H_3 + H \rightarrow C_sR_6 + C_2H_3$	2.042×10^{14}	-0.221	10.410	[38]
20	$C_sR_6{-}C_2H_3 \rightarrow C_sR_6{-}C_2H_2 + H$	3.010×10^{14}	0.340	111.255	[38]

No.	Reactions	$k = AT^n \exp(-E/RT)^a$			References
		A	n	E	
-20	$C_sR_6{-}C_2H_2 + H \rightarrow C_sR_6{-}C_2H_3$	2.184×10^{11}	0.722		[38]
21	$C_sR_6{-}C_2H_3 + H \rightarrow C_sR_6{-}C_2H_2 + H_2$	6.350×10^{04}	2.750	11.649	[38]
-21	$C_sR_6{-}C_2H_2 + H_2 \rightarrow C_sR_6{-}C_2H_3 + H$	2.509×10^{01}	3.375	3.404	[38]
22	$C_sR_6{-}C_2H_3 + OH \rightarrow C_sR_6{-}C_2H_2 + H_2O$	6.550×10^{-2}	4.200	−0.860	[38]
-22	$C_sR_6{-}C_2H_2 + H_2O \rightarrow C_sR_6{-}C_2H_3 + OH$	6.705×10^{-4}	4.613	6.162	[38]
23	$C_sR_6{-}C_2H_2 \rightarrow C_sR_6{-}C_2H_3^\bullet$	2.440×10^{30}	−5.730	32.070	[36]
-23	$C_sR_6{-}C_2H_3^\bullet \rightarrow C_sR_6{-}C_2H_2$	5.560×10^{29}	−5.620	27.910	[36]
24	$C_sR_6{-}C_2H_3^\bullet + C_2H_2 \rightarrow C_sR_6{-}R_6 + H$	3.020×10^{10}	0.702	5.530	[36]
-24	$C_sR_6{-}R_6 + H \rightarrow C_sR_6{-}C_2H_3^\bullet + C_2H_2$	1.387×10^{21}	−0.798	72.450	[36]
25	$C_sR_6{-}C_2H + H \rightarrow C_sR_6{-}C_2H_2$	1.590×10^{62}	−14.500	31.760	[36]
-25	$C_sR_6{-}C_2H_2 \rightarrow C_sR_6{-}C_2H + H$	9.003×10^{63}	−14.950	63.440	[36]
26	$C_sR_6{-}C_2H_2 + H \rightarrow C_sR_6{-}C_2H + H_2$	1.650×10^{11}	0.490	10.630	[38]
-26	$C_sR_6{-}C_2H + H_2 \rightarrow C_sR_6{-}C_2H_2 + H$	1.587×10^{09}	1.184	82.650	[38]
27	$C_sR_6{-}C_2H_2 + OH \rightarrow C_sR_6{-}C_2H + H_2O$	2.500×10^{12}			[38]
-27	$C_sR_6{-}C_2H + H_2O \rightarrow C_sR_6{-}C_2H_2 + OH$	6.230×10^{11}	0.482	87.280	[38]
28	$C_sR_6{-}C_2H + C_2H_3 \rightarrow C_sR_6{-}R_6 + H$	3.600×10^{17}	−1.440	15.758	[38]
-28	$C_sR_6{-}R_6 + H \rightarrow C_sR_6{-}C_2H + C_2H_3$	1.619×10^{29}	−3.226	74.700	[38]
29	$C_sR_6{-}C_2H^\bullet + C_2H_2 \rightarrow C_sR_6{-}R_6^\bullet$	4.490×10^{82}	−20.000	51.830	[36]
-29	$C_sR_6{-}R_6^\bullet \rightarrow C_sR_6{-}C_2H^\bullet + C_2H_2$	1.338×10^{94}	−21.840	143.500	[36]
30	$C_sR_6{-}C_2H^\bullet + C_2H_2 \rightarrow C_sR_6{-}R_6^\bullet$	1.180×10^{104}	−25.700	76.820	[36]
-30	$C_sR_6{-}R_6^\bullet \rightarrow C_sR_6{-}C_2H^\bullet + C_2H_2$	3.917×10^{115}	−27.550	168.800	[36]
31	$C_sR_6{-}C_2H^\bullet + C_2H_2 \rightarrow C_sR_6{-}R_6^\bullet$	4.490×10^{82}	−20.000	51.830	[36]
-31	$C_sR_6{-}R_6^\bullet \rightarrow C_sR_6{-}C_2H^\bullet + C_2H_2$	1.338×10^{94}	−21.840	143.500	[36]
32	$C_sR_6{-}C_2H^\bullet + C_2H_2 \rightarrow C_sR_6(C_2H)(C_2H_3) + H$	1.760×10^{40}	−7.040	48.210	[36]
-32	$C_sR_6(C_2H)(C_2H_3) + H \rightarrow C_sR_6{-}C_2H^\bullet + C_2H_2$	9.718×10^{46}	−8.438	60.840	[36]
33	$C_sR_6{-}C_2H^\bullet + C_2H_4 \rightarrow C_sR_6{-}R_6 + H$	3.620×10^{28}	−4.240	23.860	[38]
-33	$C_sR_6{-}R_6 + H \rightarrow C_sR_6{-}C_2H^\bullet + C_2H_4$	1.583×10^{40}	−6.094	87.580	[38]
34	$C_sR_6{-}C_2H_2 + C_2H_2 \rightarrow C_sR_6{-}R_6 + H$	3.570×10^{22}	−2.720	14.470	[36]
-34	$C_sR_6{-}R_6 + H \rightarrow C_sR_6{-}C_2H_2 + C_2H_2$	3.736×10^{32}	−4.109	77.230	[36]
35	$C_sR_6(C_2H)(C_2H_3) + H \rightarrow C_sR_6{-}R_6^\bullet$	1.010×10^{86}	−20.600	56.700	[36]
-35	$C_sR_6{-}R_6^\bullet \rightarrow C_sR_6(C_2H)(C_2H_3) + H$	5.450×10^{90}	−21.040	138.800	[36]
36	$C_sR_6(C_2H)(C_2H_3) + H \rightarrow C_sR_6{-}R_6^\bullet$	6.000×10^{108}	−26.600	83.590	[36]
-36	$C_sR_6{-}R_6^\bullet \rightarrow C_sR_6(C_2H)(C_2H_3) + H$	3.607×10^{113}	−27.050	162.900	[36]
	Six-member bay closure				
37	$C_sR_6{-}H + H \rightarrow C_sR_6^\bullet + H_2$	9.240×10^{07}	1.500	9.646	[43]
-37	$C_sR_6^\bullet + H_2 \rightarrow C_sR_6 + H$	9.600×10^{04}	1.960	9.021	[43]
38	$C_sR_6^\bullet \rightarrow C_sR_6{-}R_6^\bullet$	1.110×10^{11}	0.658	23.990	[43]
39	$C_sR_6^\bullet \rightarrow C_sR_6{-}R_6^\bullet$	3.490×10^{12}	−0.390	2.440	[43]
	Five-member bay closure				
40	$C_sR_6{-}H + H \rightarrow C_sR_6^\bullet + H_2$	7.250×10^{07}	1.760	9.69	[51]
-40	$C_sR_6^\bullet + H_2 \rightarrow C_sR_6 + H$	3.400×10^{09}	0.880	7.870	[51]
41	$C_sR_6^\bullet + C_sR_6{-}H \rightarrow C_sR_6^\bullet{-}C_sR_6{-}H$	3.860×10^{11}	0.210	17.700	[51]
	Phenyl addition				
42	$C_sR_6^\bullet + A_1 \rightarrow C_sR_6{-}A_1 + H$	2.220×10^{83}	−20.790	46.890	[45]
43	$C_sR_6 + A_1^\bullet \rightarrow C_sR_6{-}A_1 + H$	2.220×10^{83}	−20.790	46.890	[45]
	Five-member ring growth on a zig-zag				
44	$C_sR_6^\bullet + C_2H_2 \rightarrow C_sR_6{-}R_5 + H$	1.250×10^{27}	−3.950	16.779	[9]
45	$C_sR_6^\bullet + C_2H_2 \rightarrow C_sR_6{-}R_5 + H$	3.090×10^{20}	−2.780	8.889	[9]
46	$C_sR_6^\bullet + C_2H_2 \rightarrow C_sR_6{-}C_2H + H$	3.090×10^{25}	−3.110	31.586	[9]
47	$C_sR_6^\bullet + C_2H_2 \rightarrow C_sR_6{-}C_2H + H$	2.850×10^{7}	1.520	13.190	[9]

No.	Reactions	$k = AT^n \exp(-E/RT)^a$			References
		A	n	E	
	Five-member ring desorption				
48	$\mathrm{C_sR_5^{\bullet} \rightarrow C_sR_6{-}C_2H^{\bullet}}$	1.600×10^{14}		42.42	[7]
49	$\mathrm{C_sR_5H_2{-}C_sR_5H^{\bullet} \rightarrow C_sR_6^{\bullet} + C_2H_2}$	3.100×10^{11}	0.870	74.323	[55]
50	$\mathrm{C_sR_5H_2{-}C_sR_5H^{\bullet} \rightarrow C_sR_6{-}C_2H + H}$	6.700×10^{11}	0.840	70.790	[55]
	Five-member ring migration to a zig-zag site				
51	$\mathrm{C_sR_5H_2{-}C_sR_5H^{\bullet} \rightarrow C_sR_5H^{\bullet}{-}C_sR_5H_2}$	1.300×10^{11}	0.160	45.900	[55]
	Five-member ring migration to an armchair site				
52	$\mathrm{C_sR_5H_2{-}C_sR_5H^{\bullet} \rightarrow C_sR_6{-}C_sR_6 + H}$	1.300×10^{11}	0.160	45.900	[55]
	Partially embedded five-member ring flip reaction				
53	$\mathrm{C_sR_5H^{\bullet}{-}CsR_6 \rightarrow CsR_6{-}C_sR_5H^{\bullet}}$	1.000×10^{11}			[55, 57]
	Five-member ring conversion to six-member ring neighbouring a free-edge site				
54	$\mathrm{C_sR_6^{\bullet} + C_2H_2 \rightarrow C_sR_6{-}C_2H_2}$	1.100×10^{07}	1.610	3.896	[4]
55	$\mathrm{C_sR_6^{\bullet} + C_2H_2 \rightarrow C_sR_6{-}C_2H_2}$	3.330×10^{33}	-5.7	25.500	[4, 53]
56	$\mathrm{C_sR_5H_2{-}C_sR_5H^{\bullet} + C_s{-}C_2H \rightarrow C_sR_6}$	1.300×10^{11}	0.160	45.900	[55]
	Six-member ring conversion to five-member ring neighbouring an armchair site				
57	$\mathrm{C_sR_6^{\bullet} \rightarrow C_sR_5H_2{-}C_sR_5H^{\bullet} + C_s{-}C_2H}$	1.300×10^{11}	1.080	70.420	[7]
	Six-member ring conversion to five-member ring neighbouring a five-carbon bay site				
58	$\mathrm{C_{s-BY5}{-}C_sR_6^{\bullet} \rightarrow CsR_6{-}C_sR_5{-}C_sR_5 + H}$	2.300×10^{09}	1.603	61.850	[43]
59	$\mathrm{C_{s-BY5}{-}C_sR_6^{\bullet} \rightarrow CsR_6{-}C_sR_5{-}C_sR_5 + H}$	1.230×10^{10}	1.410	85.200	[51]
	Six-member ring desorption neighbouring a five-carbon bay site				
60	$\mathrm{C_{s-BY5}{-}C_sR_6^{\bullet} \rightarrow CsR_6{-}C_sR_6^{\bullet} + C_2H_2}$	2.300×10^{09}	1.603	61.850	[43]
	Migration of partially embedded five-member ring				
61	$\mathrm{C_sR_5{-}C_sR_5{-}C_sR_6^{\bullet} \rightarrow CsR_6^{\bullet}{-}C_sR_5{-}C_sR_5H}$	4.960×10^{11}	0.755	50.000	[51]
	Six-member ring growth on a zig-zag neighbouring a five-member ring				
62	$\mathrm{C_sR_5^{\bullet} + C_2H_2 \rightarrow CsR_5{-}R_6}$	1.235×10^{07}	1.530	9.311	[55]
	Six-member ring growth between two five-member rings				
63	$\mathrm{C_sR_5^{\bullet} + C_2H_2 \rightarrow CsR_5{-}R_6}$	1.235×10^{07}	1.530	9.311	[55]
	Five-member ring conversion to six-member ring neighbouring five-member ring				
64	$\mathrm{C_sR_5^{\bullet} + C_sR_5H \rightarrow CsR_6{-}R_5}$	8.900×10^{05}	2.280	61.489	[55]
	Six-member bay closure containing a partially embedded five-member ring				
65	$\mathrm{C_sR_6^{\bullet} \rightarrow C_sR_6{-}R_6^{\bullet}}$	1.110×10^{11}	0.658	23.990	t.w.
	Six-member ring growth on a partially embedded five-member ring armchair				
66	$\mathrm{C_sR_6{-}H + H \rightarrow C_sR_6^{\bullet} + H_2}$	2.540×10^{11}	0.931	16.440	[42]
-66	$\mathrm{C_sR_6^{\bullet} + H_2 \rightarrow C_sR_6 + H}$	1.830×10^{12}	0.397	8.815	[42]
67	$\mathrm{C_sR_6^{\bullet} + C_2H_2 \rightarrow C_sR_6{-}C_2H_2}$	1.630×10^{12}	0.409	5.675	[42]
-67	$\mathrm{C_sR_6{-}C_2H_2 \rightarrow C_sR_6^{\bullet} + C_2H_2}$	9.130×10^{11}	0.991	15.990	[42]
68	$\mathrm{C_sR_6{-}C_2H_2 \rightarrow C_sR_6^{\bullet}{-}C_2H_3}$	6.320×10^{11}	0.166	18.050	[42]
-68	$\mathrm{C_sR_6^{\bullet}{-}C_2H_3 \rightarrow C_sR_6{-}C_2H_2}$	9.750×10^{10}	0.458	15.830	[42]
69	$\mathrm{C_sR_6^{\bullet}{-}C_2H_3 \rightarrow C_sR_6H_2{-}CsR_6H^{\bullet}}$	9.580×10^{11}	-0.064	16.310	[42]
-69	$\mathrm{C_sR_6H_2{-}CsR_6H^{\bullet} \rightarrow C_sR_6^{\bullet}{-}C_2H_3}$	9.650×10^{11}	0.501	41.500	[42]
70	$\mathrm{C_sR_6H_2{-}CsR_6H^{\bullet} \rightarrow C_sR_6{-}CsR_6 + H}$	3.160×10^{12}	0.787	36.510	[42]
-70	$\mathrm{C_sR_6{-}CsR_6 + H \rightarrow C_sR_6H_2{-}CsR_6H^{\bullet}}$	9.710×10^{11}	0.507	4.695	[42]
71	$\mathrm{C_sR_6^{\bullet}{-}C_2H_3 \rightarrow C_sR_6H{-}CsR_6}$	2.780×10^{11}	0.063	23.870	[42]
-71	$\mathrm{C_sR_6H{-}CsR_6 \rightarrow C_sR_6^{\bullet}{-}C_2H_3}$	5.470×10^{11}	0.645	32.770	[42]
72	$\mathrm{C_sR_6H{-}CsR_6 \rightarrow C_sR_6{-}CsR_6 + H}$	8.150×10^{11}	0.563	24.860	[42]
-72	$\mathrm{C_sR_6{-}CsR_6 + H \rightarrow C_sR_6H{-}CsR_6}$	9.060×10^{11}	0.456	7.286	[42]
	Seven-member ring growth on a five-carbon bay site (partially embedded five-member ring)				
73	$\mathrm{C_sR_6{-}H + H \rightarrow C_sR_6^{\bullet} + H_2}$	5.897×10^{07}	1.847	17.120	[37]
-73	$\mathrm{C_sR_6^{\bullet} + H_2 \rightarrow C_sR_6 + H}$	1.215×10^{05}	2.229	7.720	[37]
74	$\mathrm{C_sR_6^{\bullet} + C_2H_2 \rightarrow C_sR_6{-}C_2H_2}$	1.348×10^{03}	2.573	4.935	[37]
-74	$\mathrm{C_sR_6{-}C_2H_2 \rightarrow C_sR_6^{\bullet} + C_2H_2}$	2.366×10^{12}	0.705	39.670	[37]

		$k = AT^n \exp(-E/RT)^a$			
No.	Reactions	A	n	E	References
75	$C_sR_6{-}C_2H_2 \rightarrow C_sR_6H{-}C_sR_6^{\bullet}$	1.958×10^{11}	0.111	25.330	[37]
-75	$C_sR_6H{-}C_sR_6^{\bullet} \rightarrow C_sR_6{-}C_2H_2$	3.412×10^{11}	0.625	53.370	[37]
76	$C_sR_6H{-}C_sR_6^{\bullet} \rightarrow C_sR_6{-}CsR_6 + H$	1.770×10^{10}	1.094	27.150	[37]
-76	$C_sR_6{-}CsR_6 + H \rightarrow C_sR_6H{-}C_sR_6^{\bullet}$	5.321×10^{07}	1.515	7.095	[37]
77	$C_sR_6{-}H + H \rightarrow C_sR_6^{\bullet} + H_2$	5.315×10^{07}	1.858	16.120	[37]
-77	$C_sR_6^{\bullet} + H_2 \rightarrow C_sR_6 + H$	9.106×10^{04}	2.277	7.007	[37]
78	$C_sR_6^{\bullet} + C_2H_2 \rightarrow C_sR_6{-}C_2H_2$	3.521×10^{03}	2.598	3.998	[37]
-78	$C_sR_6{-}C_2H_2 \rightarrow C_sR_6^{\bullet} + C_2H_2$	4.736×10^{12}	0.702	40.800	[37]
79	$C_sR_6{-}C_2H_2 \rightarrow C_sR_6H{-}C_sR_6^{\bullet}$	1.125×10^{11}	0.128	30.510	[37]
-79	$C_sR_6H{-}C_sR_6^{\bullet} \rightarrow C_sR_6{-}C_2H_2$	2.383×10^{11}	0.596	57.900	[37]
80	$C_sR_6H{-}C_sR_6^{\bullet} \rightarrow C_sR_6{-}CsR_6 + H$	1.505×10^{10}	1.076	28.840	[37]
-80	$C_sR_6{-}CsR_6 + H \rightarrow C_sR_6H{-}C_sR_6^{\bullet}$	5.841×10^{07}	1.533	7.084	[37]
	Seven-member ring growth on a five-carbon bay site (edge five-member ring)				
81	$C_sR_6{-}H + H \rightarrow C_sR_6^{\bullet} + H_2$	6.586×10^{07}	1.766	14.770	[37]
-81	$C_sR_6^{\bullet} + H_2 \rightarrow C_sR_6 + H$	1.155×10^{05}	2.310	8.819	[37]
82	$C_sR_6^{\bullet} + C_2H_2 \rightarrow C_sR_6{-}C_2H_2$	3.886×10^{03}	2.592	4.012	[37]
-82	$C_sR_6{-}C_2H_2 \rightarrow C_sR_6^{\bullet} + C_2H_2$	6.507×10^{12}	0.710	45.050	[37]
83	$C_sR_6{-}C_2H_2 \rightarrow C_sR_6H{-}C_sR_6^{\bullet}$	5.755×10^{11}	0.070	2.983	[37]
-83	$C_sR_6H{-}C_sR_6^{\bullet} \rightarrow C_sR_6{-}C_2H_2$	1.742×10^{12}	0.419	29.040	[37]
84	$C_sR_6H{-}C_sR_6^{\bullet} \rightarrow C_sR_6{-}CsR_6 + H$	3.207×10^{10}	0.958	23.130	[37]
-84	$C_sR_6{-}CsR_6 + H \rightarrow C_sR_6H{-}C_sR_6^{\bullet}$	1.293×10^{08}	1.505	7.425	[37]
85	$C_sR_5{-}H + H \rightarrow C_sR_5^{\bullet} + H_2$	1.479×10^{07}	1.854	17.070	[37]
-85	$C_sR_5^{\bullet} + H_2 \rightarrow C_sR_5 + H$	5.914×10^{04}	2.234	11.870	[37]
86	$C_sR_5^{\bullet} + C_2H_2 \rightarrow C_sR_5{-}C_2H_2$	1.098×10^{03}	2.581	7.651	[37]
-86	$C_sR_5{-}C_2H_2 \rightarrow C_sR_5^{\bullet} + C_2H_2$	2.894×10^{12}	0.709	38.300	[37]
87	$C_sR_5{-}C_2H_2 \rightarrow C_sR_5H{-}C_sR_6^{\bullet}$	5.097×10^{11}	0.139	19.740	[37]
-87	$C_sR_5H{-}C_sR_6^{\bullet} \rightarrow C_sR_5{-}C_2H_2$	9.936×10^{11}	0.410	45.260	[37]
88	$C_sR_5H{-}C_sR_6^{\bullet} \rightarrow C_sR_5{-}CsR_6 + H$	3.590×10^{11}	0.604	30.050	[37]
-88	$C_sR_5{-}CsR_6 + H \rightarrow C_sR_5H{-}C_sR_6^{\bullet}$	6.258×10^{08}	1.380	24.510	[37]
	Seven-member bay closure (H abstraction on site 1)				
89	$C_sR_6{-}H + H \rightarrow C_sR_6^{\bullet} + H_2$	3.915×10^{07}	1.876	9.421	[37]
-89	$C_sR_6^{\bullet} + H_2 \rightarrow C_sR_6 + H$	5.369×10^{04}	2.275	5.583	[37]
90	$C_sR_6^{\bullet} + C_sR_6{-}H \rightarrow C_sR_7{-}C_sR_7{-}H$	8.513×10^{11}	0.136	4.510	[37]
-90	$C_sR_7{-}C_sR_7{-}H \rightarrow C_sR_6^{\bullet} + C_sR_6{-}H$	3.523×10^{12}	0.293	25.670	[37]
91	$C_sR_7{-}C_sR_7{-}H \rightarrow C_sR_7{-}C_sR_7 + H$	2.033×10^{10}	1.067	31.600	[37]
-91	$C_sR_7{-}C_sR_7 + H \rightarrow C_sR_7{-}C_sR_7{-}H$	1.033×10^{08}	1.495	2.895	[37]
92	$C_sR_6{-}H + H \rightarrow C_sR_6^{\bullet} + H_2$	3.091×10^{07}	1.891	9.308	[37]
-92	$C_sR_6^{\bullet} + H_2 \rightarrow C_sR_6 + H$	5.144×10^{04}	2.267	7.132	[37]
93	$C_sR_6^{\bullet} + C_sR_6{-}H \rightarrow C_sR_7{-}C_sR_7{-}H$	7.041×10^{11}	0.184	10.340	[37]
-93	$C_sR_7{-}C_sR_7{-}H \rightarrow C_sR_6^{\bullet} + C_sR_6{-}H$	2.944×10^{12}	0.413	28.620	[37]
94	$C_sR_7{-}C_sR_7{-}H \rightarrow C_sR_7{-}C_sR_7 + H$	1.861×10^{10}	1.136	29.570	[37]
-94	$C_sR_7{-}C_sR_7 + H \rightarrow C_sR_7{-}C_sR_7{-}H$	7.712×10^{07}	1.514	2.067	[37]
	Seven-member bay closure (Carbene route on site 1)				
95	$C_sR_6{-}H + C_sR_6{-}H \rightarrow C_sR_6^{(2\cdot)} + C_sR_6{-}H_2$	8.031×10^{10}	0.890	95.830	[37]
-95	$C_sR_6^{(2\cdot)} + C_sR_6{-}H_2 \rightarrow C_sR_6{-}H + C_sR_6{-}H$	4.398×10^{11}	0.359	3.385	[37]
96	$C_sR_6^{(2\cdot)} + C_sR_6{-}H \rightarrow C_sR_7{-}C_sR_7{-}H$	8.031×10^{11}	0.010	8.456	[37]
-96	$C_sR_7{-}C_sR_7{-}H \rightarrow C_sR_6^{(2\cdot)} + C_sR_6{-}H$	1.897×10^{12}	0.223	17.790	[37]
97	$C_sR_7{-}H + C_sR_7 \rightarrow C_sR_7 + C_sR_7{-}H$	5.759×10^{11}	0.393		[37]
-97	$C_sR_7 + C_sR_7{-}H \rightarrow C_sR_7{-}H + C_sR_7$	1.052×10^{11}	0.905	53.500	[37]
98	$C_sR_7{-}H + C_sR_6{-}H \rightarrow C_sR_7 + C_sR_6{-}H_2 + H_2$	8.873×10^{10}	0.639	31.310	[37]
-98	$C_sR_7 + C_sR_6{-}H_2 \rightarrow C_sR_7{-}H + C_sR_6{-}H$	1.728×10^{10}	0.712	60.650	[37]

No.	Reactions	$k = AT^n \exp(-E/RT)^a$ A	n	E	References
99	$C_sR_6{-}H_2 + C_sR_6{-}H_2 \rightarrow C_sR_6{-}H + C_sR_6{-}H + H_2$	3.907×10^{09}	1.273	97.050	[37]
-99	$C_sR_6{-}H + C_sR_6{-}H + H_2 \rightarrow C_sR_6{-}H_2 + C_sR_6{-}H_2$	2.448×10^{05}	1.999	86.400	[37]
100	$C_sR_6{-}H + C_sR_6{-}H \rightarrow C_sR_6^{(2\cdot)} + C_sR_6{-}H_2$	1.061×10^{11}	0.799	84.260	[37]
-100	$C_sR_6^{(2\cdot)} + C_sR_6{-}H_2 \rightarrow C_sR_6{-}H + C_sR_6{-}H$	5.486×10^{11}	0.335	2.012	[37]
101	$C_sR_6^{(2\cdot)} + C_sR_6{-}H \rightarrow C_sR_7{-}C_sR_7{-}H$	1.000×10^{12}	-0.014	3.568	[37]
-101	$C_sR_7{-}C_sR_7{-}H \rightarrow C_sR_6^{(2\cdot)} + C_sR_6{-}H$	2.167×10^{12}	0.556	59.280	[37]
102	$C_sR_7{-}H + C_sR_6{-}H \rightarrow C_sR_7 + C_sR_6{-}H_2$	3.063×10^{11}	0.824	63.560	[37]
-102	$C_sR_7 + C_sR_6{-}H_2 \rightarrow C_sR_7{-}H + C_sR_6{-}H$	1.514×10^{10}	0.674	50.310	[37]
103	$C_sR_6{-}H_2 + C_sR_6{-}H_2 \rightarrow C_sR_6{-}H + C_sR_6{-}H + H_2$	4.479×10^{09}	0.714	27.100	[37]
-103	$C_sR_6{-}H + C_sR_6{-}H + H_2 \rightarrow C_sR_6{-}H_2 + C_sR_6{-}H_2$	2.332×10^{05}	1.742	55.100	[37]
	Seven-member bay closure (H abstraction on site 2)				
104	$C_sR_6{-}H + H \rightarrow C_sR_6^{\bullet} + H_2$	2.767×10^{07}	1.913	9.542	[37]
-104	$C_sR_6^{\bullet} + H_2 \rightarrow C_sR_6 + H$	4.212×10^{04}	2.264	6.878	[37]
105	$C_sR_6^{\bullet} + C_sR_6{-}H \rightarrow C_sR_7{-}C_sR_7{-}H$	4.703×10^{11}	0.143	4.722	[37]
-105	$C_sR_7{-}C_sR_7{-}H \rightarrow C_sR_6^{\bullet} + C_sR_6{-}H$	1.476×10^{12}	0.367	27.37	[37]
106	$C_sR_7{-}C_sR_7{-}H \rightarrow C_sR_7{-}C_sR_7 + H$	6.424×10^{09}	1.093	32.16	[37]
-106	$C_sR_7{-}C_sR_7 + H \rightarrow C_sR_7{-}C_sR_7{-}H$	1.693×10^{08}	1.522	1.637	[37]
107	$C_sR_6{-}H + H \rightarrow C_sR_6^{\bullet} + H_2$	2.843×10^{07}	1.906	9.533	[37]
-107	$C_sR_6^{\bullet} + H_2 \rightarrow C_sR_6 + H$	5.338×10^{04}	2.261	7.525	[37]
108	$C_sR_6^{\bullet} + C_sR_6{-}H \rightarrow C_sR_7{-}C_sR_7{-}H$	6.599×10^{11}	0.082	2.625	[37]
-108	$C_sR_7{-}C_sR_7{-}H \rightarrow C_sR_6^{\bullet} + C_sR_6{-}H$	5.132×10^{12}	0.340	25.40	[37]
109	$C_sR_7{-}C_sR_7{-}H \rightarrow C_sR_7{-}C_sR_7 + H$	2.006×10^{10}	1.099	32.81	[37]
-109	$C_sR_7{-}C_sR_7 + H \rightarrow C_sR_7{-}C_sR_7{-}H$	1.729×10^{08}	1.489	1.504	[37]
	Seven-member bay closure (Carbene route on site 2)				
110	$C_sR_6{-}H + C_sR_6{-}H \rightarrow C_sR_6^{(2\cdot)} + C_sR_6{-}H_2$	1.603×10^{11}	0.777	83.23	[37]
-110	$C_sR_6^{(2\cdot)} + C_sR_6{-}H_2 \rightarrow C_sR_6{-}H + C_sR_6{-}H$	3.050×10^{11}	0.294		[37]
111	$C_sR_6^{(2\cdot)} + C_sR_6{-}H \rightarrow C_sR_7{-}C_sR_7{-}H$	2.488×10^{11}	0.120	11.62	[37]
-111	$C_sR_7{-}C_sR_7{-}H \rightarrow C_sR_6^{(2\cdot)} + C_sR_6{-}H$	1.472×10^{12}	0.676	45.09	[37]
112	$C_sR_7{-}H + C_sR_7 \rightarrow C_sR_7 + C_sR_7{-}H$	1.397×10^{11}	0.581	27.01	[37]
-112	$C_sR_7 + C_sR_7{-}H \rightarrow C_sR_7{-}H + C_sR_7$	3.264×10^{10}	0.734	56.81	[37]
113	$C_sR_7{-}H + C_sR_6{-}H \rightarrow C_sR_7 + C_sR_6{-}H_2 + H_2$	5.515×10^{10}	0.849	59.32	[37]
-113	$C_sR_7 + C_sR_6{-}H_2 \rightarrow C_sR_7{-}H + C_sR_6{-}H$	7.566×10^{10}	0.675	38.56	[37]
114	$C_sR_6{-}H_2 + C_sR_6{-}H_2 \rightarrow C_sR_6{-}H + C_sR_6{-}H + H_2$	6.206×10^{09}	0.848	28.61	[37]
-114	$C_sR_6{-}H + C_sR_6{-}H + H_2 \rightarrow C_sR_6{-}H_2 + C_sR_6{-}H_2$	2.164×10^{05}	1.798	58.70	[37]
115	$C_sR_6{-}H + C_sR_6{-}H \rightarrow C_sR_6^{(2\cdot)} + C_sR_6{-}H_2$	1.162×10^{11}	0.837	86.01	[37]
-115	$C_sR_6^{(2\cdot)} + C_sR_6{-}H_2 \rightarrow C_sR_6{-}H + C_sR_6{-}H$	4.948×10^{11}	0.331	1.476	[37]
116	$C_sR_6^{(2\cdot)} + C_sR_6{-}H \rightarrow C_sR_7{-}C_sR_7{-}H$	5.744×10^{11}	0.039	8.721	[37]
-116	$C_sR_7{-}C_sR_7{-}H \rightarrow C_sR_6^{(2\cdot)} + C_sR_6{-}H$	2.164×10^{12}	0.292	18.61	[37]
117	$C_sR_7{-}H + C_sR_6{-}H \rightarrow C_sR_7 + C_sR_6{-}H_2$	9.900×10^{11}	0.331	-2.850	[37]
-117	$C_sR_7 + C_sR_6{-}H_2 \rightarrow C_sR_7{-}H + C_sR_6{-}H$	1.025×10^{11}	0.875	57.11	[37]
118	$C_sR_7{-}H + C_sR_6{-}H \rightarrow C_sR_7 + C_sR_6{-}H_2 + H_2$	6.156×10^{10}	0.782	39.25	[37]
-118	$C_sR_7 + C_sR_6{-}H_2 \rightarrow C_sR_7{-}H + C_sR_6{-}H$	9.567×10^{10}	0.696	35.20	[37]
119	$C_sR_6{-}H_2 + C_sR_6{-}H_2 \rightarrow C_sR_6{-}H + C_sR_6{-}H + H_2$	3.478×10^{09}	1.288	87.43	[37]
-119	$C_sR_6{-}H + C_sR_6{-}H + H_2 \rightarrow C_sR_6{-}H_2 + C_sR_6{-}H_2$	1.696×10^{05}	2.086	95.63	[37]

[a]*The units are mole, centimetre, second, and kilocalorie.*

[b]*Low-pressure limit in TROE form. Parameters* $A = 0.70546, T_3 = 9.999E+09, T_1 = 459.918, T_2 = -8.214E+09$

[c]*The reverse rate coefficients were calculated via equilibrium constants.*

Table S2: *Kinetic Monte Carlo jump processes*

Process [Ref.]	Parent site
S1 Free-edge ring growth [4]	**Free-edge (FE)**

Jump Process:

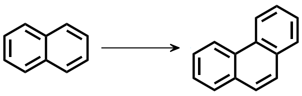

Rate[a]:

$$\left(k_{18}[C_sR_6^{\bullet}][C_4H_4]+k_{24}[C_sR_6{-}C_2H_3^{\bullet}][C_2H_2]+k_{28}[C_sR_6{-}C_2H][C_2H_3]+k_{29}[C_sR_6{-}C_2H^{\bullet}][C_2H_2]+k_{30}[C_sR_6{-}C_2H^{\bullet}][C_2H_2]+k_{31}[C_sR_6{-}C_2H^{\bullet}][C_2H_2]+k_{33}[C_sR_6{-}C_2H^{\bullet}][C_4H_4]+k_{34}[C_sR_6{-}C_2H_2][C_2H_2]+k_{35}[C_sR_6(C_2H)(C_2H_3)][H]+k_{36}[C_sR_6(C_2H)(C_2H_3)][H]\right)[C_{FE}]$$

S2 Armchair ring growth [4]	**Armchair (AC)**

Jump Process:

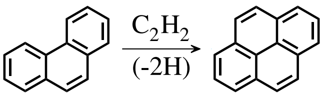

Rate:

$$(k_9+k_{10})\left(\frac{k_1[H]+k_2[OH]}{k_{-1}[H_2]+k_3[H]+k_{-2}[H_2O]+(k_9+k_{10}+k_{11}+k_{12})[C_2H_2]}\right)[C_2H_2][C_{AC}]$$

S3 Free-edge desorption to an armchair [9, 38]	**Armchair (AC)**

Jump Process:

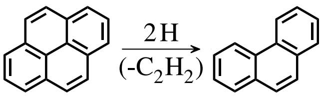

Rate:

$$(k_{-9}+k_{-10})[C_{FE}]$$

S4 Free-edge ring desorption [4]	**Free-edge with two adjacent free-edges (FE3)**

Jump Process:

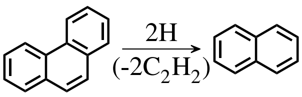

Rate:

$$\left(k_{-18}+k_{-24}+k_{-28}+k_{-33}+k_{-34}+k_{-35}\right)[H][C_{FE3}] + \left(\frac{(k_1[H]+k_2[OH])(k_{-29}+k_{-30}+k_{-31})}{k_{-1}[H_2]+k_3[H]+k_{-2}[H_2O]}\right)[C_{FE3}]$$

S5 6- to 5-member ring conversion at armchair [4]	**Armchair next to FE3 (AC_{FE3})**

Jump Process:

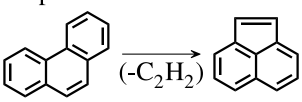

Rate:

$$k_{57}\left(\frac{k_1[H]+k_2[OH]}{k_{-1}[H_2]+k_3[H]+k_{-2}[H_2O]+k_{57}}\right)[C_{AC_{FE3}}]$$

S6 5-member ring addition [4]	**Zig-zag (ZZ)**

Jump Process:

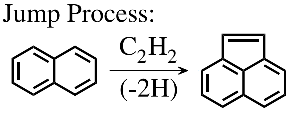

Rate:

$$(k_{44}+k_{45})\left(\frac{k_1[H]+k_2[OH]}{k_{-1}[H_2]+k_3[H]+k_{-2}[H_2O]+(k_{44}+k_{45}+k_{46}+k_{47})[C_2H_2]}\right)[C_2H_2][C_{ZZ}]$$

Process [Ref.]	Parent site
S7 5-member ring desorption [4]	**5-member ring (R5)**

Jump Process:

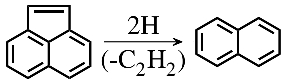

Rate:

$$\left(\frac{k_{48}(k_4[\mathrm{H}]+k_5[\mathrm{OH}])}{k_{-4}[\mathrm{H_2}]+k_6[\mathrm{H}]+k_{-5}[\mathrm{H_2O}]+k_{48}}+\frac{k_7[\mathrm{H}](k_{49}+k_{50})}{k_{-7}[\mathrm{H}]+k_8[\mathrm{H}]+k_{49}+k_{50}}\right)[\mathrm{C_{R5}}]$$

S8 5- to 6-member ring conversion at free edge [4]	**5-member ring next to free-edge (RFE)**

Jump Process:

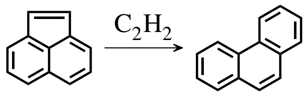

Rate:

$$(k_{54}+k_{55})\left(\frac{k_7[\mathrm{H}]}{k_{-7}[\mathrm{H}]+k_8[\mathrm{H}]+k_{49}+k_{50}+k_{51}+(k_{54}+k_{55})f[\mathrm{C_2H_2}]}\right)f[\mathrm{C_2H_2}][\mathrm{C_{RFE}}],$$

$$\text{where } f=\left(\frac{k_1[\mathrm{H}]+k_2[\mathrm{OH}]}{k_{-1}[\mathrm{H_2}]+k_3[\mathrm{H}]+k_{-2}[\mathrm{H_2O}]+(k_{54}+k_{55})[\mathrm{C_2H_2}]}\right)$$

S9 5- to 6-member ring conversion at armchair [4]	**5-member ring next to armchair (RAC)**

Jump Process:

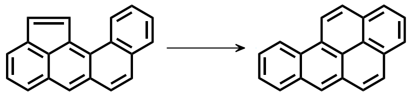

Rate:

$$k_{52}\left(\frac{k_7[\mathrm{H}]}{k_{-7}[\mathrm{H}]+k_8[\mathrm{H}]+k_{49}+k_{50}+k_{51}+k_{52}}\right)[\mathrm{C_{RAC}}]$$

S10 Benzene addition [43]	**All site types**

Jump Process:

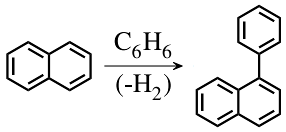

Rate:

$$2k_{42}\left(\frac{k_1[\mathrm{H}]+k_2[\mathrm{OH}]}{k_{-1}[\mathrm{H_2}]+k_3[\mathrm{H}]+k_{-2}[\mathrm{H_2O}]+k_{42}[\mathrm{C_6H_6}]}\right)[\mathrm{C_6H_6}][\mathrm{C_s}]$$

S11 5-member ring migration [43]	**5-member ring next to zig-zag (RZZ)**

Jump Process:

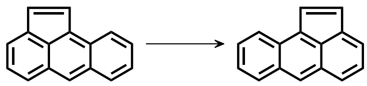

Rate:

$$k_{51}\left(\frac{k_7[\mathrm{H}]}{k_{-7}[\mathrm{H}]+k_8[\mathrm{H}]+k_{49}+k_{50}+k_{51}}\right)[\mathrm{C_{RZZ}}]$$

S12 Ring growth next to 5-member ring [55]	**5-member ring next to zig-zag (RZZ)**

Jump Process:

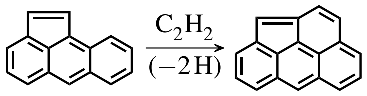

Rate:

$$k_{62}\left(\frac{k_1[\mathrm{H}]+k_2[\mathrm{OH}]}{k_{-1}[\mathrm{H_2}]+k_3[\mathrm{H}]+k_{-2}[\mathrm{H_2O}]+k_{62}[\mathrm{C_2H_2}]}+\frac{k_4[\mathrm{H}]+k_5[\mathrm{OH}]}{k_{-4}[\mathrm{H_2}]+k_6[\mathrm{H}]+k_{-5}[\mathrm{H_2O}]+k_{62}[\mathrm{C_2H_2}]}\right)[\mathrm{C_{RZZ}}]$$

Process [Ref.]	Parent site
S13 Ring growth between 5-member rings [55]	**Free-edge between 5-member rings (RFER)**

Jump Process:

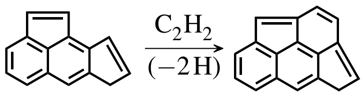

Rate:

$$k_{63}\left(\frac{k_4[H]+k_5[OH]}{k_{-4}[H_2]+k_6[H]+k_{-5}[H_2O]+k_{63}[C_2H_2]}\right)[C_{RFER}]$$

S14 5-member rings collision [55]	**Zig-zag between 5-member rings (RZZR)**

Jump Process:

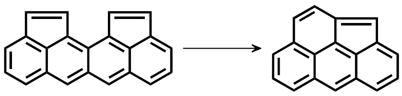

Rate:

$$2k_{64}\left(\frac{k_7[H]}{k_{-7}[H]+k_8[H]+k_{49}+k_{50}+k_{64}}\right)[C_{RZZR}]$$

S15 6-member bay closure [43]	**6-member bay (BY6)**

Jump Process:

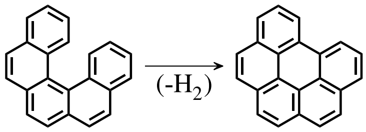

Rate:

$$2(k_{38}+k_{39})\left(\frac{k_{37}[H]+k_2[OH]}{k_{-37}[H_2]+k_3[H]+k_{-2}[H_2O]+k_{38}+k_{39}}\right)[C_{BY6}]$$

S16 5-member bay closure [43]	**5-member bay (BY5)**

Jump Process:

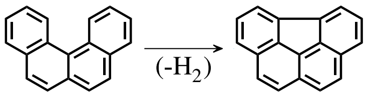

Rate:

$$2k_{41}\left(\frac{k_{40}[H]+k_2[OH]}{k_{-40}[H_2]+k_3[H]+k_{-2}[H_2O]+k_{41}}\right)[C_{BY5}]$$

S17 6-member bay closure [43] **(partially embedded 5-member ring)**	**6-member bay ($BY6_{eR5}$) with partially embedded 5-member ring**

Jump Process:

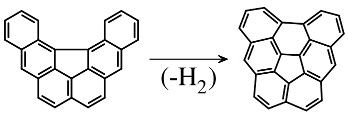

Rate:

$$2k_{65}\left(\frac{k_{37}[H]+k_2[OH]}{k_{-37}[H_2]+k_3[H]+k_{-2}[H_2O]+k_{65}}\right)[C_{BY6_{eR5}}]$$

S18 Partially embedded 5-member ring migration [43]	**Partially embedded 5-member ring (eR5)**

Jump Process:

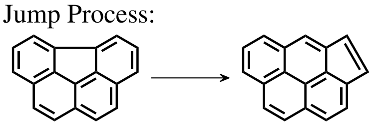

Rate:

$$k_{61}\left(\frac{k_3[H]+k_2[OH]}{k_{-1}[H_2]+k_3[H]+k_{-2}[H_2O]+k_{61}}\right)[C_{eR5}]$$

S19 6-member ring desorption at bay [44]	**BY5 next to FE3 ($BY5_{FE3}$)**

Jump Process:

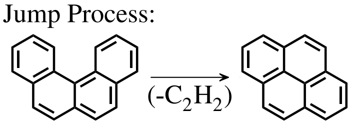

Rate:

$$k_{60}\left(\frac{k_1[H]+k_2[OH]}{k_{-1}[H_2]+k_3[H]+k_{-2}[H_2O]+k_{60}}\right)[C_{BY5_{FE3}}]$$

Process [Ref.]	Parent site
S20 6-member ring rearrangement at bay [44]	**BY5 next to FE3 ($BY5_{FE3}$)**

Jump Process:

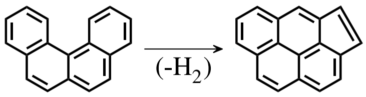

Rate:

$$(k_{58}+k_{59})\left(\frac{k_1[H]+k_2[OH]}{k_{-1}[H_2]+k_3[H]+k_{-2}[H_2O]+k_{58}+k_{59}}\right)[C_{BY5_{FE3}}]$$

Process [Ref.]	Parent site
S21 Capping of embedded 5-member ring[42]	**Embedded 5-member ring (eR5)**

Jump Process:

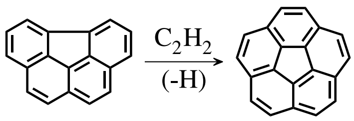

Rate[b]:

$$(k_{70}[C_sR_6H_2]_{ss}+k_{72}[C_sR_6H-C_sR_6]_{ss})\,[C_{eR5}]$$

Process [Ref.]	Parent site
S22 7-member ring growth [this work] (edge 5-member ring)	**5-member ring next to 5-member bay (RBY5)**

Jump Process:

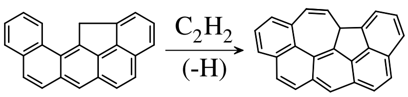

Rate[c]:

$$(k_{84}[C_sR_6H-C_sR_6^{\bullet}]_{ss}+k_{88}[C_sR_5H-C_sR_6^{\bullet}]_{ss})\,[C_{RBY5}]$$

Process [Ref.]	Parent site
S23 7-member ring growth [this work] (partially embedded 5-member ring)	**5-member bay ($BY5_{eR5}$) with partially embedded 5-member ring**

Jump Process:

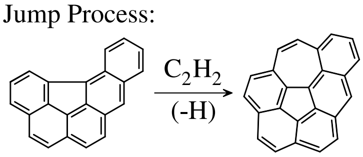

Rate[d]:

$$(k_{76}[C_sR_6H-C_sR_6^{\bullet}]_{ss}+k_{80}[C_sR_6H-C_sR_6{}^{\bullet}{}_{i}]_{ss})\,[C_{BY5_{eR5}}]$$

Process [Ref.]	Parent site
S24 7-member bay closure [this work] (partially embedded 5-member ring 1)	**7-member bay site 1($BY7_{eR5-1}$) with partially embedded 5-member ring**

Jump Process:

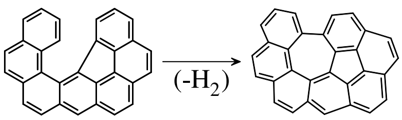

Rate[e]:

$$(k_{91}[C_sR_7-C_sR_7-H]_{ss}+k_{94}[C_sR_7-C_sR_7-H_i]_{ss}+ k_{99}[C_sR_6H_2-C_sR_6H_2]_{ss}+k_{103}[C_sR_6H_2-C_sR_6H_{2i}]_{ss})\,[C_{BY7_{eR5-1}}]$$

Process [Ref.]	Parent site
S25 7-member bay closure [this work] (partially embedded 5-member ring 2)	**7-member bay site 2($BY7_{eR5-2}$) with partially embedded 5-member ring**

Jump Process:

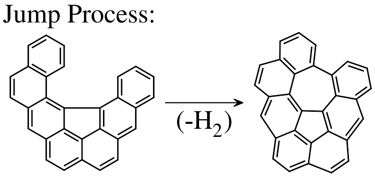

Rate[f]:

$$(k_{106}[C_sR_7-C_sR_7-H]_{ss}+k_{109}[C_sR_7-C_sR_7-H_i]_{ss}+ k_{114}[C_sR_6H_2-C_sR_6H_2]_{ss}+k_{119}[C_sR_6H_2-C_sR_6H_{2i}]_{ss})\,[C_{BY7_{eR5-2}}]$$

Notes:
[a]Steady-state intermediates vector V_{ss} and Partial-equilibrium intermediates vector V_{peq} defined as:
$V_{ss} = \{C_sR_6^\bullet, C_sR_6{-}C_2H_2, C_sR_6{-}C_2H, C_sR_6{-}C_2H_3, C_sR_6{-}C_2H_3^\bullet, C_sR_6(C_2H)(C_2H_3), C_sR_6{-}R_6^\bullet, C_sR_6{-}R_6\}$
$V_{peq} = \{C_sR_6^\bullet, C_sR_6{-}C_2H_2, C_sR_6{-}C_2H, C_sR_6{-}C_2H_3, C_sR_6{-}C_2H_3^\bullet, C_sR_6(C_2H)(C_2H_3)\}$
Rate calculated as per Leon et al. [28]: $\dot{r}_{S1} = \dot{r}_{S1,ss}$ if $\dot{r}_{S1,peq} > \dot{r}_{S3}$, $\dot{r}_{S1} = \dot{r}_{S1,peq}$ o.w.
[b]Steady-state intermediates vector V_{ss} defined as:
$V_{ss} = \{C_sR_6^\bullet, C_sR_6{-}C_2H_2, C_sR_6^\bullet{-}C_2H_3, C_sR_6{-}H_2, C_sR_6H{-}C_sR_6\}$
[c]Steady-state intermediates vector V_{ss} defined as:
$V_{ss} = \{C_sR_6^\bullet, C_sR_6{-}C_2H_2, C_sR_6H{-}C_sR_6^\bullet, C_sR_5^\bullet, C_sR_5{-}C_2H_2, C_sR_5H{-}C_sR_6^\bullet\}$
[d]Steady-state intermediates vector V_{ss} defined as:
$V_{ss} = \{C_sR_6^\bullet, C_sR_6{-}C_2H_2, C_sR_6H{-}C_sR_6^\bullet, C_sR_6{}^\bullet{}_i, C_sR_6{-}C_2H_{2i}, C_sR_6H{-}C_sR_6{}^\bullet{}_i\}$
[e]Steady-state intermediates vector V_{ss} defined as:
$V_{ss} = \{C_sR_6^\bullet, C_sR_7{-}R_7{-}H, C_sR_6{}^\bullet{}_i, C_sR_7{-}R_7{-}H_i, C_sR_6^{2\bullet}, C_sR_7H{-}C_sR_7, C_sR_7H{-}C_sR_6H, C_sR_6{}^{2\bullet}{}_i, C_sR_7H{-}C_sR_{7i}, C_sR_7H{-}C_sR_6H_i\}$
[f]Steady-state intermediates vector V_{ss} defined as:
$V_{ss} = \{C_sR_6^\bullet, C_sR_7{-}R_7{-}H, C_sR_6{}^\bullet{}_i, C_sR_7{-}R_7{-}H_i, C_sR_6^{2\bullet}, C_sR_7H{-}C_sR_7, C_sR_7H{-}C_sR_6H, C_sR_6{}^{2\bullet}{}_i, C_sR_7H{-}C_sR_{7i}, C_sR_7H{-}C_sR_6H_i\}$

S2.2 Assumptions on process rates

S2.2.1 Hydrogen abstraction

- By H atom.
  Rate constants were taken from Semenikhin et al. [48] for the abstraction of hydrogen from benzene.

- By OH radical.
  Taken from Kislov et al. [24].

- By H addition.
  Taken from Harding et al. [15].

- Abstractions from five-member rings.
  Taken from Hou and You [18]. Abstractions by OH radical assumed similar to those from six-member rings.

S2.2.2 Armchair growth

Rate constants taken from Frenklach et al. [9] for the formation of pyrene from phenanthrene. It was assumed that the process competes with the formation of the ethynylphenanthrene to other products.

S2.2.3 Free-edge desorption to produce an armchair

Rate constants taken from Frenklach et al. [9] for the formation of pyrene from phenanthrene. Reverse rate constants equations were fitted using the thermal data developed by [38].

S2.2.4 Free-edge growth

Rate constants taken from the network of reactions described by Mebel et al. [36] for different pressures. The case for 1 atm is used in this work. For additional reactions not included in that work, like the reactions with C_2H_3 and C_4H_4, the reactions were taken from Narayanaswamy et al. [38] for the intermediate species between benzene and naphthalene. The equations were solved using a combined partial-equilibrium and steady-state methodology as defined by Leon et al. [28]. For the ring-growth process rate the reactions are evaluated in the forward direction. If the partial-equilibrium rate is larger than the consumption rate (evaluating the reactions in the reverse direction) then the steady-state rate is selected. See again Leon et al. [28].

S2.2.5 Six-member ring desorption

The desorption uses the same rate constants as the free-edge growth jump process [36, 38]. However, it uses the reverse reactions from naphthalene losing a ring to produce benzene. The PAH radicals that proceed to a ring opening were assumed to be in a partial-equilibrium with the PAH and the hydrogen abstraction reactions.

S2.2.6 Six-member bay closure

The rate constants for this process were calculated at the B3LYP/6-311+G(d,p) level of theory (see main text). These rate constants were similar to those of Raj et al. [43].

S2.2.7 Five-member bay closure

The rate constants for this process were taken from Violi [51].

S2.2.8 Phenyl addition

The rate constants for this process were taken from Richter et al. [45]. Two pathways were considered, the direct addition of the phenyl group and the reaction between the PAH radical and a benzene molecule. The concentrations of both phenyl radical and PAH radical were assumed to be in steady-state with hydrogen abstractions and phenyl additions.

S2.2.9 Five-member ring growth on a zig-zag

Rate constants taken from Frenklach et al. [9] for the formation of acenaphthylene. It was assumed that the process competes with the formation of ethynylnaphthalene to other products.

S2.2.10 Five-member ring desorption

Two routes were assumed for the desorption of a five-member ring: First, an hydrogen abstraction followed by bond dissociation similar to Frenklach et al. [7]. For the second route it was assumed that an hydrogen addition step would be followed by a competition of five-member ring migration and desorption as proposed by Whitesides and Frenklach [55].

S2.2.11 Five-member ring migration to a zig-zag site

Rate constants taken from Whitesides and Frenklach [55]. A steady-state approximation was assumed for the five-member ring addition intermediate.

S2.2.12 Five-member ring migration to neighbouring armchair site

Rate constants taken from Whitesides and Frenklach [55]. A steady-state approximation was assumed for the five-member ring addition intermediate.

S2.2.13 Partially embedded five-member ring flip reaction

Rate constants taken from Whitesides and Frenklach [55] and Whitesides et al. [57].

S2.2.14 Conversion of six-member ring to five-member ring neighbouring a zig-zag site

Rate constants taken from Celnik et al. [4]. A steady-state approximation was assumed for the short-lived intermediate.

S2.2.15 Conversion of five-member ring to six-member ring neighbouring a free-edge

Rate constants taken from Celnik et al. [4]. A steady-state approximation was assumed for the short-lived intermediate.

S2.2.16 Conversion of six-member ring neighbouring an armchair site

Rate constants taken from Frenklach et al. [7]. A steady-state approximation was assumed for the short-lived intermediate.

S2.2.17 Conversion of six-member ring to five-member ring next a five-carbon-bay site

Rate constants taken from Raj et al. [43] and Violi [51].

S2.2.18 Migration of partially embedded five-member ring

The migration rate was taken from Violi [51]. The migration equilibrium constant was taken from Whitesides and Frenklach [55] allowing migrations between internal zigzag edges to be equally probable. Migrations of a partially-embedded five membered ring to an edge were assumed to have probability of one third. Migrations of an edge five membered ring to the zigzag edge were assumed to have two thirds probability.

S2.2.19 Six-member ring growth on a zig-zag site neighbouring a five-member ring

Rate constants taken from Whitesides and Frenklach [55]. A steady-state approximation was assumed for the six-member ring addition intermediate.

S2.2.20 Six-member ring growth between two five-member rings

Rate constants taken from Whitesides and Frenklach [55]. A steady-state approximation was assumed for the six-member ring addition intermediate.

S2.2.21 Six-member bay closure containing a partially embedded five-member ring

The rate constants for this process were calculated at the B3LYP/6-311+G(d,p) level of theory (see main text).

S2.2.22 Six-member ring growth on armchair containing a partially embedded five-member ring

The rate constants for this process were taken from Raj [42] (see main text).

S2.2.23 Seven-member ring growth on a five-carbon-bay site containing a partially embedded five-member ring

The rates constants were taken from Menon et al. [37] (see main text).

S2.2.24 Seven-member bay closure

The rates constants were taken from Menon et al. [37] (see main text).

S3 Animations showing the growth of example PAHs

Animated files showing the growth of example PAHs are provided via the University of Cambridge data repository (Link to be provided).

References

[1] B. Apicella, P. Pré, M. Alfè, A. Ciajolo, V. Gargiulo, C. Russo, A. Tregrossi, D. Deldique, and J. Rouzaud. Soot nanostructure evolution in premixed flames by high resolution electron transmission microscopy (HRTEM). *Proc. Combust. Inst.*, 35(2):1895–1902, 2015. doi:https://doi.org/10.1016/j.proci.2014.06.121.

[2] M. L. Botero, Y. Sheng, J. Akroyd, J. Martin, J. A. Dreyer, W. Yang, and M. Kraft. Internal structure of soot particles in a diffusion flame. *Carbon*, 141:635–642, 2019. doi:https://doi.org/10.1016/j.carbon.2018.09.063.

[3] K. Bowal, J. W. Martin, A. J. Misquitta, and M. Kraft. Ion-induced soot nucleation using a new potential for curved aromatics. *Combust. Sci. Technol.*, 191(5-6):747–765, 2019. doi:10.1080/00102202.2019.1565496.

[4] M. Celnik, A. Raj, R. West, R. Patterson, and M. Kraft. Aromatic site description of soot particles. *Combust. Flame*, 155(1-2):161–180, 2008. doi:10.1016/j.combustflame.2008.04.011.

[5] M. Commodo, K. Kaiser, G. D. Falco, P. Minutolo, F. Schulz, A. D'Anna, and L. Gross. On the early stages of soot formation: Molecular structure elucidation by high-resolution atomic force microscopy. *Combust. Flame*, 205:154–164, 2019. doi:https://doi.org/10.1016/j.combustflame.2019.03.042.

[6] A. D'Anna, A. Violi, A. D'Alessio, and A. F. Sarofim. A reaction pathway for nanoparticle formation in rich premixed flames. *Combust. Flame*, 127(1):1995–2003, 2001. doi:10.1016/S0010-2180(01)00303-0.

[7] M. Frenklach, C. A. Schuetz, and J. Ping. Migration mechanism of aromatic-edge growth. *Proc. Combust. Inst.*, 30(1):1389–1396, 2005. doi:https://doi.org/10.1016/j.proci.2004.07.048.

[8] M. Frenklach, Z. Liu, R. I. Singh, G. R. Galimova, V. N. Azyazov, and A. M. Mebel. Detailed, sterically-resolved modeling of soot oxidation: Role of O atoms, interplay with particle nanostructure, and emergence of inner particle burning. *Combust. Flame*, 188:284–306, 2018. doi:https://doi.org/10.1016/j.combustflame.2017.10.012.

[9] M. Frenklach, R. I. Singh, and A. M. Mebel. On the low-temperature limit of HACA. *Proc. Combust. Inst.*, 37(1):969–976, 2019. doi:https://doi.org/10.1016/j.proci.2018.05.068.

[10] P. Gerhardt, S. Löffler, and K. Homann. Polyhedral carbon ions in hydrocarbon flames. *Chem. Phys. Lett.*, 137(4):306–310, 1987. doi:https://doi.org/10.1016/0009-2614(87)80889-8.

[11] D. G. Goodwin, R. L. Speth, H. K. Moffat, and B. W. Weber. Cantera: An object-oriented software toolkit for chemical kinetics, thermodynamics, and transport processes. https://www.cantera.org, 2018. Version 2.4.0.

[12] W. J. Grieco, J. B. Howard, L. C. Rainey, and J. B. V. Sande. Fullerenic carbon in combustion-generated soot. *Carbon*, 38(4):597–614, 2000. doi:https://doi.org/10.1016/S0008-6223(99)00149-9.

[13] J. Guo, J. R. Morris, Y. Ihm, C. I. Contescu, N. C. Gallego, G. Duscher, S. J. Pennycook, and M. F. Chisholm. Topological defects: Origin of nanopores and enhanced adsorption performance in nanoporous carbon. *Small*, 8(21):3283–3288, 2012. doi:10.1002/smll.201200894.

[14] N. Hansen, M. Schenk, K. Moshammer, and K. Kohse-Höinghaus. Investigating repetitive reaction pathways for the formation of polycyclic aromatic hydrocarbons in combustion processes. *Combust. Flame*, 180:250–261, 2017. ISSN 0010-2180. doi:https-//doi.org/10.1016/j.combustflame.2016.09.013. URL http://www.sciencedirect.com/science/article/pii/S0010218016302620.

[15] L. B. Harding, Y. Georgievskii, and S. J. Klippenstein. Predictive theory for hydrogen atom-hydrocarbon radical association kinetics. *J. Phys. Chem. A*, 109(21):4646–4656, 2005. doi:10.1021/jp0508608.

[16] P. J. F. Harris. Fullerene-like models for microporous carbon. *J. Mater. Sci.*, 48(2):565–577, Jan 2013. doi:10.1007/s10853-012-6788-1.

[17] K.-H. Homann. Fullerenes and soot formation - New pathways to large particles in flames. *Angew. Chem. Int. Ed. Engl.*, 37(18):2435–2451, 1998.

[18] D. Hou and X. You. Reaction kinetics of hydrogen abstraction from polycyclic aromatic hydrocarbons by H atoms. *Phys Chem Chem Phys.*, 19:30772–30780, 2017. doi:10.1039/C7CP04964A.

[19] J. B. Howard. Carbon addition and oxidation reactions in heterogeneous combustion and soot formation. *Proc. Combust. Inst.*, 23(1):1107–1127, 1991.

[20] P. Y. Huang, C. S. Ruiz-Vargas, A. M. van der Zande, W. S. Whitney, M. P. Levendorf, J. W. Kevek, S. Garg, J. S. Alden, C. J. Hustedt, Y. Zhu, J. Park, P. L. McEuen, and D. A. Muller. Grains and grain boundaries in single-layer graphene atomic patchwork quilts. *Nature*, 469(7330):389–392, 2011. doi:10.1038/nature09718.

[21] C. Irimiea, A. Faccinetto, X. Mercier, I.-K. Ortega, N. Nuns, E. Therssen, P. Desgroux, and C. Focsa. Unveiling trends in soot nucleation and growth: When secondary ion mass spectrometry meets statistical analysis. *Carbon*, 144:815–830, 2019. doi:10.1016/j.carbon.2018.12.015.

[22] K. Johansson, M. Head-Gordon, P. Schrader, K. Wilson, and H. Michelsen. Resonance-stabilized hydrocarbon-radical chain reactions may explain soot inception and growth. *Science*, 361(6406):997–1000, 2018.

[23] K. O. Johansson, T. Dillstrom, P. Elvati, M. F. Campbell, P. E. Schrader, D. M. Popolan-Vaida, N. K. Richards-Henderson, K. R. Wilson, A. Violi, and H. A. Michelsen. Radical–radical reactions, pyrene nucleation, and incipient soot formation in combustion. *Proc. Combust. Inst.*, 36(1):799–806, 2017. doi:https://doi.org/10.1016/j.proci.2016.07.130.

[24] V. V. Kislov, N. I. Islamova, A. M. Kolker, S. H. Lin, and A. M. Mebel. Hydrogen abstraction acetylene addition and Diels-Alder mechanisms of PAH formation: A detailed study using first principles calculations. *J. Chem. Theory Comput.*, 1(5): 908–924, 2005. doi:10.1021/ct0500491.

[25] V. V. Kislov, A. I. Sadovnikov, and A. M. Mebel. Formation mechanism of polycyclic aromatic hydrocarbons beyond the second aromatic ring. *J. Phys. Chem. A*, 117(23):4794–4816, 2013. doi:10.1021/jp402481y.

[26] H. W. Kroto. The stability of the fullerenes Cn, with n = 24, 28, 32, 36, 50, 60 and 70. *Nature*, 329(6139):529–531, 1987. doi:10.1038/329529a0.

[27] A. L. Lafleur, J. B. Howard, K. Taghizadeh, E. F. Plummer, L. T. Scott, A. Necula, and K. C. Swallow. Identification of C20H10 dicyclopentapyrenes in flames: Correlation with corannulene and fullerene formation. *J. Phys. Chem.*, 100(43): 17421–17428, 1996. doi:10.1021/jp9605313.

[28] G. Leon, N. Eaves, J. Akroyd, S. Mosbach, and M. Kraft. A new methodology to calculate process rates in a Kinetic Monte Carlo model of PAH growth. *Combust. Flame*, 209:133–143, 2019. doi:https://doi.org/10.1016/j.combustflame.2019.07.032.

[29] S. lijima, T. Ichihashi, and Y. Ando. Pentagons, heptagons and negative curvature in graphite microtubule growth. *Nature*, 356(6372):776–778, 1997. doi:10.1038/356776a0.

[30] J. W. Martin, R. I. Slavchov, E. K. Y. Yapp, J. Akroyd, S. Mosbach, and M. Kraft. The polarization of polycyclic aromatic hydrocarbons curved by pentagon incorporation: The role of the flexoelectric dipole. *J. Phys. Chem. C*, 121(48):27154–27163, 2017. doi:10.1021/acs.jpcc.7b09044.

[31] J. W. Martin, M. Botero, R. I. Slavchov, K. Bowal, J. Akroyd, S. Mosbach, and M. Kraft. Flexoelectricity and the formation of carbon nanoparticles in flames. *J. Phys. Chem. C*, 122(38):22210–22215, 2018. doi:10.1021/acs.jpcc.8b08264.

[32] J. W. Martin, K. Bowal, A. Menon, R. I. Slavchov, J. Akroyd, S. Mosbach, and M. Kraft. Polar curved polycyclic aromatic hydrocarbons in soot formation. *Proc. Combust. Inst.*, 37(1):1117–1123, 2019. doi:https://doi.org/10.1016/j.proci.2018.05.046.

[33] J. W. Martin, C. de Tomas, I. Suarez-Martinez, M. Kraft, and N. A. Marks. Topology of disordered 3D graphene networks. *Phys. Rev. Lett.*, 123:116105, Sep 2019. doi:10.1103/PhysRevLett.123.116105.

[34] J. W. Martin, D. Hou, A. Menon, J. Akroyd, X. You, and M. Kraft. Reactivity of polycyclic aromatic hydrocarbon radicals: Implications for soot formation. *J. Phys. Chem. C*, 123(43):26673, 2019.

[35] J. W. Martin, A. Menon, C. T. Lao, J. Akroyd, and M. Kraft. Dynamic polarity of curved aromatic soot precursors. *Combust. Flame*, 206:150–157, 2019. doi:https://doi.org/10.1016/j.combustflame.2019.04.046.

[36] A. M. Mebel, Y. Georgievskii, A. W. Jasper, and S. J. Klippenstein. Temperature- and pressure-dependent rate coefficients for the HACA pathways from benzene to naphthalene. *Proc. Combust. Inst.*, 36(1):919–926, 2017. doi:https-//doi.org/10.1016/j.proci.2016.07.013.

[37] A. Menon, G. Leon, J. Akroyd, and M. Kraft. A density functional theory study on the formation of 7-member rings in polyaromatic hydrocarbons. *Combust. Flame, submitted*, 2019.

[38] K. Narayanaswamy, G. Blanquart, and H. Pitsch. A consistent chemical mechanism for oxidation of substituted aromatic species. *Combust. Flame*, 157(10):1879–1898, 2010. doi:https://doi.org/10.1016/j.combustflame.2010.07.009.

[39] A. I. Podlivaev and L. A. Openov. Dynamics of the Stone-Wales defect in graphene. *Phys. Solid State*, 57(4):820–824, Apr 2015. doi:10.1134/S1063783415040265.

[40] C. J. Pope, J. A. Marr, and J. B. Howard. Chemistry of fullerenes C60 and C70 formation in flames. *J. Phys. Chem.*, 97(42):11001–11013, 1993. doi:10.1021/j100144a018.

[41] S. H. Pun and Q. Miao. Toward negatively curved carbons. *Acc. Chem. Res.*, 51(7): 1630–1642, 2018. doi:10.1021/acs.accounts.8b00140.

[42] A. Raj. Structural effects on the growth of large polycyclic aromatic hydrocarbons by C2H2. *Combust. Flame*, 204:331–340, 2019. ISSN 0010-2180. doi:https://doi.org/10.1016/j.combustflame.2019.03.027.

[43] A. Raj, M. Celnik, R. Shirley, M. Sander, R. Patterson, R. West, and M. Kraft. A statistical approach to develop a detailed soot growth model using PAH characteristics. *Combust. Flame*, 156(4):896–913, 2009. doi:10.1016/j.combustflame.2009.01.005.

[44] A. Raj, P. L. Man, T. S. Totton, M. Sander, R. A. Shirley, and M. Kraft. New polycyclic aromatic hydrocarbon (PAH) surface processes to improve the model prediction of the composition of combustion-generated PAHs and soot. *Carbon*, 48(2):319 – 332, 2010. doi:https://doi.org/10.1016/j.carbon.2009.09.030.

[45] H. Richter, S. Granata, W. H. Green, and J. B. Howard. Detailed modeling of PAH and soot formation in a laminar premixed benzene/oxygen/argon low-pressure flame. *Proc. Combust. Inst.*, 30(1):1397–1405, 2005. ISSN 1540-7489. doi:j.proci.2004.08.088.

[46] A. W. Robertson and J. H. Warner. Atomic resolution imaging of graphene by transmission electron microscopy. *Nanoscale*, 5:4079–4093, 2013. doi:10.1039/C3NR00934C.

[47] M. Schenk, L. Leon, K. Moshammer, P. Oßwald, T. Zeuch, L. Seidel, F. Mauss, and K. Kohse-Höinghaus. Detailed mass spectrometric and modeling study of isomeric butene flames. *Combust. Flame*, 160(3):487–503, 2013. ISSN 0010-2180. doi:https-//doi.org/10.1016/j.combustflame.2012.10.023. URL http-//www.sciencedirect.com/science/article/pii/S0010218012003112.

[48] A. S. Semenikhin, A. S. Savchenkova, I. V. Chechet, S. G. Matveev, Z. Liu, M. Frenklach, and A. M. Mebel. Rate constants for H abstraction from benzo(a)pyrene and chrysene: A theoretical study. *Phys Chem Chem Phys.*, 19:25401–25413, 2017. doi:10.1039/C7CP05560A.

[49] R. Singh and M. Frenklach. A mechanistic study of the influence of graphene curvature on the rate of high-temperature oxidation by molecular oxygen. *Carbon*, 101: 203–212, 2016. doi:https://doi.org/10.1016/j.carbon.2016.01.090.

[50] S. A. Skeen, H. A. Michelsen, K. R. Wilson, D. M. Popolan, A. Violi, and N. Hansen. Near-threshold photoionization mass spectra of combustion-generated high-molecular-weight soot precursors. *J. Aerosol Sci.*, 58:86–102, 2013. doi:https://doi.org/10.1016/j.jaerosci.2012.12.008.

[51] A. Violi. Cyclodehydrogenation reactions to cyclopentafused polycyclic aromatic hydrocarbons. *J. Phys. Chem. A*, 109(34):7781–7787, 2005. doi:10.1021/jp052384r.

[52] C. Wang, T. Huddle, C.-H. Huang, W. Zhu, R. L. V. Wal, E. H. Lester, and J. P. Mathews. Improved quantification of curvature in high-resolution transmission electron microscopy lattice fringe micrographs of soots. *Carbon*, 117:174–181, 2017. doi:https://doi.org/10.1016/j.carbon.2017.02.059.

[53] H. Wang and M. Frenklach. Calculations of rate coefficients for the chemically activated reactions of acetylene with vinylic and aromatic radicals. *JPhysChem*, 98 (44):11465–11489, 1994. doi:10.1021/j100095a033.

[54] Q. Wang, P. Elvati, D. Kim, K. O. Johansson, P. E. Schrader, H. A. Michelsen, and A. Violi. Spatial dependence of the growth of polycyclic aromatic compounds in an ethylene counterflow flame. *Carbon*, 149:328–335, 2019. doi:https://doi.org/10.1016/j.carbon.2019.03.017.

[55] R. Whitesides and M. Frenklach. Detailed Kinetic Monte Carlo simulations of graphene-edge growth. *J. Phys. Chem. A*, 114(2):689–703, 2010. doi:10.1021/jp906541a.

[56] R. Whitesides and M. Frenklach. Effect of reaction kinetics on graphene-edge morphology and composition. *Z. fur Phys. Chem.*, 229(4):597–614, 2015. doi:10.1515/zpch-2014-0633.

[57] R. Whitesides, D. Domin, R. Salomón-Ferrer, W. A. Lester, and M. Frenklach. Graphene layer growth chemistry: Five- and six-member ring flip reaction. *J. Phys. Chem. A*, 112(10):2125–2130, 2008. doi:10.1021/jp075785a.

[58] X.-Z. Wu, Y.-R. Yao, M.-M. Chen, H.-R. Tian, J. Xiao, Y.-Y. Xu, M.-S. Lin, L. Abella, C.-B. Tian, C.-L. Gao, Q. Zhang, S.-Y. Xie, R.-B. Huang, and L.-S. Zheng. Formation of curvature subunit of carbon in combustion. *J. Am. Chem. Soc.*, 138(30):9629–9633, 2016. doi:10.1021/jacs.6b04898.

[59] E. K. Yapp, C. G. Wells, J. Akroyd, S. Mosbach, R. Xu, and M. Kraft. Modelling PAH curvature in laminar premixed flames using a detailed population balance model. *Combust. Flame*, 176:172–180, 2017. doi:10.1016/j.combustflame.2016.10.004.

[60] X. You, R. Whitesides, D. Zubarev, W. A. Lester, and M. Frenklach. Bay-capping reactions: Kinetics and influence on graphene-edge growth. *Proc. Combust. Inst.*, 33(1):685–692, 2011. doi:https://doi.org/10.1016/j.proci.2010.05.110.